NOTICE

The quality of this microform is heavily dependent upon the quality of the original thesis submitted for microfilming. Every effort has been made to ensure the highest quality of reproduction possible.

If pages are missing, contact the university which granted the degree.

Some pages may have indistinct print especially if the original pages were typed with a poor typewriter ribbon or if the university sent us an inferior photocopy.

Reproduction in full or in part of this microform is governed by the Canadian Copyright Act, R.S.C. 1970, c. C-30, and subsequent amendments.

AVIS

La qualité de cette microforme dépend grandement de la qualité de la thèse soumise au microfilmage. Nous avons tout fait pour assurer une qualité supérieure de reproduction.

S'il manque des pages, veuillez communiquer avec l'université qui a conféré le grade.

La qualité d'impression de certaines pages peut laisser à désirer, surtout si les pages originales ont été dactylographiées à l'aide d'un ruban usé ou si l'université nous a fait parvenir une photocopie de qualité inférieure.

La reproduction, même partielle, de cette microforme est soumise à la Loi canadienne sur le droit d'auteur, SRC 1970, c. C-30, et ses amendements subséquents.

UNIVERSITY OF ALBERTA

DEVELOPMENT AND EXPERIMENTAL VALIDATION OF INSTABILITY THEORY FOR IMMISCIBLE DISPLACEMENTS IN CYLINDRICAL SYSTEMS

by

Chayan Chakrabarty

A THESIS

SUBMITTED TO THE FACULTY OF GRADUATE STUDIES AND RESEARCH IN PARTIAL FULFILLMENT OF THE REQUIREMENTS FOR THE DEGREE OF

Master of Science in

PETROLEUM ENGINEERING

DEPARTMENT OF MINING, METALLURGICAL AND PETROLEUM ENGINEERING

EDMONTON, ALBERTA

Spring, 1990

NOTICE

The quality of this microform is heavily dependent upon the quality of the original thesis submitted for microfilming. Every effort has been made to ensure the highest quality of reproduction possible.

If pages are missing, contact the university which granted the degree.

Some pages may have indistinct print especially if the original pages were typed with a poor typewriter ribbon or if the university sent us an inferior photocopy.

Reproduction in full or in part of this microform is governed by the Canadian Copyright Act, R.S.C. 1970, c. C-30, and subsequent amendments.

AVIS

La qualité de cette microforme dépend grandement de la qualité de la thèse soumise au microfilmage. Nous avons tout fait pour assurer une qualité supérieure de reproduction.

S'il manque des pages, veuillez communiquer avec l'université qui a conféré le grade.

La qualité d'impression de certaines pages peut laisser à désirer, surtout si les pages originales ont été dactylographiées à l'aide d'un ruban usé ou si l'université nous a fait parvenir une photocopie de qualité inférieure.

La reproduction, même partielle, de cette microforme est soumise à la Loi canadienne sur le droit d'auteur, SRC 1970, c. C-30, et ses amendements subséquents.

ISBN 0-315-60300-3

MICRO

UNIVERSITY OF ALBERTA

RELEASE FORM

NAME OF AUTHOR Chayan Chakrabarty

TITLE OF THESIS **DEVELOPMENT AND EXPERIMENTAL VALIDATION OF INSTABILTY THEORY FOR IMMISCIBLE DISPLACEMENTS IN CYLINDRICAL SYSTEMS**

DEGREE FOR WHICH THESIS WAS PRESENTED Master of Science

YEAR THIS DEGREE GRANTED 1990

(SIGNED) Chayan Chakrabarty

PERMANENT ADDRESS: c/o MR. B. CHAKRABARTY
21 T.S. FLAT, P.O. KADMA
JAMSHEDPUR - 831005,
INDIA .

DATED APRIL 12, 1990

THE UNIVERSITY OF ALBERTA

FACULTY OF GRADUATE STUDIES AND RESEARCH

The undersigned certify that they have read, and recommend to the Faculty of Graduate Studies and Research, for acceptance, a thesis entitled **DEVELOPMENT AND EXPERIMENTAL VALIDATION OF INSTABILITY THEORY FOR IMMISCIBLE DISPLACEMENTS IN CYLINDRICAL SYSTEMS** submitted by Chayan Chakrabarty in partial fulfillment of the requirements for the degree of Master of Science in PETROLEUM ENGINEERING.

R.G.Bentsen Supervisor

T.Spanos

W.H.Griffin

A.K.Ambastha

D.L.Flock

J.M.Whiting

Date: March 30, 1990

TO

MY PARENTS

ABSTRACT

Viscous fingering can reduce significantly the displacement efficiency when one fluid immiscibly displaces another in a porous medium. As a consequence, it is of importance to be able to predict whether a displacement is stable or unstable. A stability theory for linear displacement in cylindrical systems, assuming a moving boundary model and the utilization of a force potential approach, is presented in this study. The theory is validated by comparing experimental results with those obtained theoretically.

Twenty-one experiments, using two different viscosity ratios, have been performed in cylindrical unconsolidated porous media. It is demonstrated that the theory predicts correctly the onset of instability for immiscible displacement in cylindrical systems. By means of photographing different sections of the core, the location along the length of the core where fingering began has been identified. This technique helped demonstrate that the theory can be used to predict the breakthrough recovery for both stable and pseudostable displacements.

Also presented in this study is a statistical sensitivity analysis pertaining to the calculations of the instability number and the breakthrough recovery. By means of this analysis, it is possible to identify the experimental variables which most contribute to the total bias and variance in the calculations of the instability number and the breakthrough recovery. Also, an estimate has been made of the effect of the variability resulting from the properties of the sand and the packing procedure on the total experimental variability.

ACKNOWLEDGEMENT

I am grateful to Dr. R.G. Bentsen for his supervision, guidance and encouragement extended throughout the course of this study. I am also indebted to Prof. W.H. Griffin for his continued help and advice throughout the period of this study. Thanks are also due to Dr. J. M. Whiting, Dr. D.L. Flock, Dr. A.K. Ambastha and Dr. T. Spanos for their valuable comments and suggestions.

I specially thank Mrs. Barbara Bentsen who kindly reviewed the manuscript and Mrs. Darlene Spelten who painstakingly typed the thesis. The thesis could not have been completed without Mr. Robert Smith, who designed the coreholder used in this study, Mr. John Czuroski, who processed the photographs taken during the course of this study and Mr. Jacques Gibeau, who offered countless helpful suggestions at various stages of this study.

I am also grateful to the Natural Sciences and Engineering Research Council of Canada and to the Alberta Oil Sands Technology and Research Authority for the financial assistance which made this study possible. Also, thanks are extended to Imperial Oil Limited for providing the oils used in this study.

Last, but not least, I with to thank Romita for her warm support, continued encouragement, understanding and patience.

TABLE OF CONTENTS

LIST OF TABLES

LIST OF FIGURES

LIST OF PHOTOGRAPHIC PLATES

NOMENCLATURE

a	Core radius, m [ft]
a_o, a_w	Initial amplitudes of disturbance for oil and water fingers, respectively, m [ft]
A	System cross-sectional area, m^2 [ft^2]
A_c	Area under capillary pressure curve, kPa [psi]
A_{sw}	Surface area of water finger, m^2 [ft^2]
C	Factor depending only on the nature of the porous media, m^{-1} [ft^{-1}]
C_1, C_2	Arbitrary constants of proportionality in Equation 28
$C(M)$	Correction factor, function of mobility ratio
$C_c(M)$	Correction factor for cylindrical systems, defined by Equation 85
$C_r(M)$	Correction factor for rectangular systems, defined by Equation 86
d_{1l}	First order partial derivative of the function $f(X_1, X_2, ..., X_n)$ at a point distant h to the left of the point of interest, given by Equation 132
d_{1r}	First order partial derivative of the function $f(X_1, X_2, ..., X_n)$ at a point distant h to the right of the point of interest, given by Equation 133
d_2	Second order partial derivative of the function $f(X_1, X_2, ..., X_n)$ at the point of interest, given by Equation 134
D	Core diameter, m [ft]
$E[X_i]$	The expected value of variable X_i
f	Value of the function $f(X_1, X_2, ..., X_n)$ at the point of interest
f_{m1}	Value of the function $f(X_1, X_2, ..., X_n)$ at a point distant h to the left of the point of interest
f_{m2}	Value of the function $f(X_1, X_2, ..., X_n)$ at a point distant 2h to the left of the point of interest
f_{P1}	Value of the function $f(X_1, X_2, ..., X_n)$ at a point distant h to the right of the point of interest

f_{P_2}	Value of the function $f(X_1, X_2, ..., X_n)$ at a point distant 2h to the right of the point of interest
g	Gravitational acceleration, m/s^2 [ft/sec^2]
h	The spacing interval as a function of the standard deviation of the variable of interest, given by Equation 130
IOIP	Initial Oil in Place, m^3 [ft^3]
I_{sc}	Instability number for cylindrical systems
J_n	Bessel Function of order n
K	Absolute permeability of a sandpack, m^2 [d]
K_{oiw}	Permeability to oil at initial water saturation, m^2 [d]
K_{wor}	Permeability to water at residual oil saturation, m^2 [d]
L	Length of the porous medium, m [ft]
m	Mode number
M	Endpoint mobility ratio
n	A positive integer giving a qualitative indication of the number of fingers
n_w	Time constant, sec^{-1}
N_c	Capillary number
N_g	Gravitational number
P_c (t)	Microscopic capillary pressure, kPa [psi]
$(P_{co})_w$	Macroscopic capillary pressure in the region where water is flowing, kPa [psi]
$(P_{cw})_o$	Macroscopic capillary pressure in the region where oil is flowing, kPa [psi]
$(P_{co})_{oc}$	Equilibrium macroscopic capillary pressure in the region where oil is flowing, kPa [psi]
Q	Volumetric injection rate, m^3/s [ft^3/sec]
Q_o, Q_w	Stabilized flow rates of oil and water, respectively, m^3/s [ft^3/sec]

r	Radial coordinate, m [ft]
$R(r)$	Separated function for finger surface, given by Equation 29
R_{bt}	Breakthrough recovery, fraction of IOIP
R_{sw}	Rate at which new surface is being created, m^2/s [ft^2/sec]
S_{or}	Residual oil saturation
S_y	Estimation of the standard deviation of variable y
t	Real time, sec
t_o	Time after commencement of injection when the fingering starts, sec
v	Superficial velocity, m/s [ft/sec]
v_a	Average velocity of a stable displacement front, m/s [ft/sec]
$(v^*_{om})_w$	Maximal velocity of propagation of an oil finger, m/s [ft/sec]
v_{or}, $v_{o\theta}$, v_{oz}	r, θ, and z components of oil superficial velocity vector, respectively, m/s [ft/sec]
$(v^*_{or})_w$, $(v^*_{o\theta})_w$, $(v^*_{oz})_w$	Oil perturbation velocities in the r, θ and z directions, respectively, in the region where water is flowing, m/s [ft/sec]
v_{wa}	Average rate at which water crosses the base of a water finger, m/s [ft/sec]
v_{wfa}	Actual velocity of a water finger, m/s [ft/sec]
$(v^*_{wm})_o$	Maximal velocity of propagation of a water finger, m/s [ft/sec]
v_{wr}, $v_{w\theta}$, v_{wz}	r, θ, and z components of water superficial velocity vector, respectively, m/s [ft/sec]
$(v^*_{wr})_o$, $(v^*_{w\theta})_o$, $(v^*_{wz})_o$	Water perturbation velocities in the r, θ, and z directions, respectively, in the region where oil is flowing, m/s [ft/sec]
VAR (y)	Variance of the variable y
V_b	Bulk volume of the sandpack, m^3 [ft^3]

V_o	Volume of an oil finger, m^3 [ft^3]
V_p	Pore volume of the sandpack, m^3 [ft^3]
V_w	Volume of a water finger, m^3 [ft^3]
z	Z-direction in the cylindrical coordinate system, m [ft]
z_o	Amplitude of an oil finger, m [ft]
z_w	Amplitude of a water finger, m [ft]
Z_o	Location where fingering commenced, m [ft]
α	Angle core makes with the vertical, radians [degrees]
α_m	The m^{th} root of Equation 49
β_w	Constant of proportionality, given by Equation 74
γ_c	Characteristic eigenvalue for which capillary and gravity forces exactly balance viscous forces, m^{-1} [ft^{-1}]
γ_o, γ_w	Eigenvalues for oil and water regions, respectively, m^{-1} [ft^{-1}]
$(\eta_w)_o$	Function for the surface of a water finger in the region where oil is flowing, as defined by Equation 47, m [ft]
θ	Angular direction in cylindrical coordinates, radians [degrees]
$\Theta(\theta)$	Separated function for finger surface, given by Equation 27
λ_w	Wavelength of a water finger, m [ft]
ξ	Function for the surface of a finger, m [ft]
$(\xi_o)_w$	Function for the surface of an oil finger in the region where water is flowing, m [ft]
$(\xi_w)_o$	Function for the surface of a water finger in the region where oil is flowing, as defined by Equation 30, m [ft]
μ	Separation constant, given in Equation 22
μ_o, μ_w	Oil and water viscosities, respectively, Pa-s [cp]
ρ_o, ρ_w	Oil and water densities, respectively, kg/m^3 [g/cm^3]
$\Delta\rho$	Water-oil density contrast, kg/m^3 [g/cm^3]

Σ	Summation
σ	Interfacial tension, mN/m [dyne/cm]
σ_e	Pseudointerfacial tension, mN/m [dyne/cm]
σ_{GP}	Variability due to geological properties of the sand and the packing procedure in the estimation of instability number and breakthrough recovery
σ_M	Variability due to measurement of the component variables in the estimation of instability number and breakthrough recovery
σ_T	Total variability in the estimation of instability number and breakthrough recovery, as given by Equation 136
ϕ	Porosity, fraction
Φ	Force potential, N·m/kg [lbf-ft/lbm]
Φ_c	Capillary potential, N·m/kg [lbf-ft/lbm]
Φ_{oi}	Initial value of the potential in oil on the oil side of the interface, N·m/kg [lbf-ft/lbm]
Φ_{wi}	Initial value of the potential in water on the water side of the interface, N·m/kg [lbf-ft/lbm]
$(\Phi_w^*)_o$	Perturbation potential for water in the region where only oil is flowing, N·m/kg [lbf-ft/lbm]
$(\Phi_w)_w$	Water force potential in the region where only water is flowing, N·m/kg [lbf-ft/lbm]
$\rightarrow$	Vector notation
∇	Gradient operator

1. INTRODUCTION

With the ever-increasing demand for energy, it is of prime importance to be able to improve efficiencies of existing recovery methods. Waterflooding has been the most important secondary recovery method used for decades. Hence, research effort aimed at gaining more insight into the various factors governing recovery efficiencies of waterflood projects could be of immense importance.

Two of the more important factors governing the efficiency of any immiscible displacement process are the heterogeneity of the reservoir and the displacement stability. While man has no control over the scale and distribution of the heterogeneities in the system, he does have control over some of the parameters governing the stabilty of the displacement process. The stability of an immiscible displacement process depends upon the balance of viscous, gravitational and capillary forces which exist in the system. If the viscous forces exceed gravitational and capillary forces, the system becomes unstable, and viscous fingers develop. Thus, it is of importance to be able to predict if a displacement is stable or unstable.

There are two usual approaches to determining the conditions for instability in immiscible displacements. The first approach uses first-order perturbation analysis and the concept of a velocity potential. This theoretical approach, however, can deal only with the incipient finger, as first-order perturbation theory is valid only if the perturbations are small. Moreover, a velocity potential exists only for fields of flow involving a fluid having constant viscosity and density and a homogeneous and isotropic porous medium. Thus, such an approach should not be applied when the flow is taking place in a real porous medium.

The second approach uses the Buckley-Leverett displacement equations. However, a major limitation associated with theories following this approach is that they make use of conventional relative permeability and capillary pressure curves which

are valid only for stable displacements. Hence, the usefulness of the application of these theories to unstable displacements is debatable.

Another approach to identifying the stability boundary during immiscible displacements in porous media has been developed recently. This analysis does not suffer from the limitations associated with the previous approaches. This theory is based on the assumption of a moving boundary model and uses the concept of a force potential. The theory, which has been developed for rectangular-shaped porous media, has been validated experimentally. However, a similar theory for immiscible displacements in cylindrical systems has yet to be developed.

2. LITERATURE REVIEW

It has long been recognized that the identification of the nature of an immsicible displacement process, that is, whether it is stable or unstable, has practical and theoretical value. Consequently, a number of authors have attempted to derive the theory necessary to predict the conditions which give rise to instability during the immiscible displacement of one fluid by another in a porous medium. These theories can be classified into two broad groups: theories based on the Buckley-Leverett displacement model and theories based on the moving boundary model. Most of the theories based on the Buckley-Leverett model have met with only partial success, mainly because of mathematical complications. On the other hand, theories based on the moving boundary model have been successful not only in identifying the stability boundary, but also in predicting breakthrough recoveries for stable and pseudostable displacements.

2.1 Buckley-Leverett models

Rachford [1] was the first author to develop a stability theory based on the Buckley-Leverett equations. He argued that the performance of waterfloods in parallel-plate models differed significantly from that of waterfloods in water-wet porous systems containing connate water. Such differences were related primarily to how saturation was distributed and to mobility ratio. Hence, he suggested that stability theories based on parallel-plate models were not appropriate for predicting the instability of immiscible displacement in porous media. Introducing perturbations in capillary pressure and in the average pressure and using the Buckley-Leverett model, he proposed a set of partial differential equations governing these perturbations. However, the non-linearity of the equations forced him to assume the ten saturation-dependent coefficients of the equations to be constant. Also, he used numerical techniques based on a few select initial peturbations to obtain solutions to the equations. Rachford observed that the presence of a saturation transition zone behind the invading

front in a waterflood greatly modified the fingering phenomena in water-wet systems. He observed no tendency towards fingering in all the cases he studied for connate-water bearing systems. He also concluded from his studies that increasing the water-oil mobility difference decreased the tendency toward instability. However, Rachford's findings are questionable because of the simplifying assumptions he made, which have been discussed previously. Also, it is possible that other instability processes (dispersion effects, etc.) might have been present in the cases that he studied.

In 1974, Hagoort [2] also investigated the stability of immiscible displacements in water-wet porous media containing connate water by using the Buckley-Leverett model. Arguing that the Muskat model of oil-water displacement was not valid for displacements in water-wet porous media, he concluded from his analysis that it was the so-called shock mobility ratio, which is lower than the end-point mobility ratio, which governed the stability of a Buckley-Leverett-type displacement. Neglecting gravitational forces, he showed that, in the absence of capillary forces, displacements were unstable when the mobility ratio of the fluids behind and ahead of the shock front was greater than one. Hagoort assumed that capillarity determined the wavelength of an instability and, hence, included in his analysis the influence of capillary forces, using energy arguments. His theory, though devoid of the existence of a critical wavelength, assumed that the most dominant wavelength in an unstable displacement would be the one associated with maximal energy dissipation. He concluded that a displacement would be unstable if the shock mobility ratio were greater than one, provided that the most probable wavelength was smaller than the width of the porous medium. However, it is noteworthy that Hagoort, in order to simplify the analytical computation, assumed that the flow consisted of two zones of constant saturation, separated by a narrow transition zone. It can be seen from his analysis that for his theory to be valid for moderate-to-high values of mobility ratio, the above-mentioned assumption should approach that of a moving boundary displacement.

Yortsos and Huang [3] used multiphase flow principles to conduct a linear stability analysis of the steady-state velocity, saturation and pressure distributions for immiscible, two-phase displacement processes, by taking into account two-phase flow on both sides of the front. They found that capillarity had a strong stabilizing influence on flow disturbances. However, in the absence of capillary effects, flow stability was shown to depend on the contrast in total mobility. The concept of total mobility contrast was also used by Jerauld et al. [4] in their recent treatment where they showed that, in the absence of gravity, the fronts were stable when the total mobility of the flowing fluids far ahead of the front was greater than that of those flowing far behind the front.

Theories which employ Buckley-Leverett type equations in the stability analysis present some significant problems. In all the approaches mentioned above, except that of Hagoort [2], the perturbation equations are solved numerically. Numerical methods generally have numerical dispersion and numerical instabilities associated with them, the effects of which may be difficult to distinguish from the actual behaviour of the displacement system. Also, all of these theories make use of conventional relative-permeability and capillary-pressure curves which are valid only for displacements that are stable in nature. Thus, the use of these curves to predict the behaviour of an unstable displacement is questionable.

2.2 Moving boundary models

In 1950, Taylor [5] used small-perturbation analysis to study the stability of a planar interface between two superimposed fluids of different densities when accelerated in a direction normal to the interface. Neglecting the effects of viscosity and interfacial tension, Taylor showed, using first-order theory, that the interface was stable or unstable for small perturbations according to whether the acceleration was directed from the more dense to the less dense fluid or vice versa. In a subsequent study, Lewis

[6] conducted a series of experiments which demonstrated the validity of Taylor's theory.

Taking into account both gravity and viscosity effects, Hill [7] developed a theory to account for the channelling which sometimes occurs when one fluid displaces another along a uniformly packed column. He was able to define a critical velocity in terms of the viscosities and densities of the two fluids. He showed that, depending on the relation between the actual and the critical velocities, displacements can be stable or unstable. For example, when water displaced a denser and more viscous liquid, channelling occurred whenever the velocity of flow exceeded the critical velocity.

The above-mentioned phenomena of channelling of a displacing fluid through a displaced fluid under certain flow conditions were observed by Engelberts and Klinkenberg [8], who coined the term "viscous fingering". They carried out a series of laboratory experiments on the displacement of oil by water in a homogeneous porous medium. It was concluded that when the driving fluid was more mobile than the driven fluid, the interface between the two fluids would become unstable, and this instability would result in a severe decrease in recovery efficiency. They identified viscosity ratio and rate of displacement as the important factors controlling the "fingering" phenomenon. Engelberts and Klinkenberg observed that at a viscosity ratio of one the displacing fluid uniformly invaded the porous medium and the breakthrough recovery increased with the displacement rate. At higher viscosity ratios, the porous medium was relatively well-invaded at low displacement rates. At high rates, the displacement was haphazard and large sections of the porous medium were uncontacted by the displacing water. For a given rate of displacement, the breakthrough recovery was observed to be much lower for a higher viscosity ratio displacement and also, for a viscosity ratio greater than one, the breakthrough recovery fell off significantly as the rate was increased.

Similar conclusions were arrived at by van Meurs [9] in 1957. He studied the mechanisms of flow processes using a three-dimensional transparent model that permitted direct visual observations of the displacement process. He studied the influence of viscosity ratio on the displacement efficiency of a linear waterdrive both in a homogeneous formation and in a stratified formation,and also on the displacement efficiency of a waterflood using a five-spot well pattern. By means of photography of the displacement process at different stages of the experiment, he was able to show that there was virtually no fingering when the oil-water viscosity ratio was equal to one, whereas at a viscosity ratio of 80, water invasion occurred in the form of well-defined fingers.

The study conducted by van Meurs [9] did not include an investigation of the effects of surface tension on interfacial instability. Bellman and Pennington [10] were the first authors to include the effects of viscosity in a stability analysis. They studied the influence of surface tension and viscosity on the formation, and rate of growth, of Taylor instability. They concluded that the introduction of viscosity eliminated instability of the interface for small wavelength disturbances. They also observed that the instability when both viscosity and surface tension were accounted for was less than that when only viscosity was present. That is, surface tension was found to have a stabilizing influence on the flow disturbances at the interface.

Results similar to those found by Taylor [5] were obtained by Saffman and Taylor [11] in a study conducted in 1958. Assuming that two immiscible fluids remain completely separated along a planar interface, the authors investigated the flow stability in a Hele-Shaw cell. They concluded that when the two viscous fluids flowed in a direction perpendicular to the interface, the interface was stable or unstable to small perturbations depending on whether the direction of motion was from the less-mobile to the more-mobile fluid or vice versa, irrespective of the relative densities of the fluids, provided that the displacement rate was large enough. They also studied the effect of

surface tension on stability of motion in a Hele-Shaw cell. They concluded that surface tension limited the range of disturbances which were unstable to those characterized by wavelengths greater than a critical value which was a function of the surface tension, the plate separation, the flow velocity and the differences between the densities and viscosities of the two fluids.

In a study, similar to that of Saffman and Taylor [11], Chuoke et al. [12] presented a systematic theoretical analysis of viscous fingering from the stability viewpoint. Their theory, published in 1959, is considered to be one of the most important on the subject of linear instability in immiscible displacements in Hele-Shaw models. In developing this theory, Chuoke et al. postulated the existence of a velocity potential and assumed a piston-like displacement model and a porous medium that was macroscopically homogeneous and isotropic throughout. Their analytical study, based on a first-order linear perturbation analysis of the immiscible displacement of one fluid by another, allowed them to derive the necessary and sufficient conditions for instability. According to them, for instability to occur, the displacement rate had to be greater than a critical value, and the perturbed displaced front had to contain wavelengths of disturbance greater than a critical value which resulted from the interfacial tension between the two immiscible fluids. By examining the sinusoidal frontal distortion of each wavelength, they found that a different initial growth rate occurred for each wavelength. They then reasoned that the fastest growing wavelength will dominate the displacement process and will have a peak-to-peak separation of $\sqrt{3}$ times the critical wavelength. Their theoretical development was validated by experiments conducted in Hele-Shaw cells.

In 1962, Outmans [13] attempted to improve the first-order theory for frontal stability that had been developed by Saffman and Taylor [11] and Chuoke et al. [12] by utilizing non-linear perturbation theory. His extended first-order theory, he suggested, could describe correctly the growth and shape of the viscous fingers. Using the

method of higher-order approximation, he solved the non-linear stability problem, including in his solutions perturbations up to the fourth degree. He showed that the simple relationship between interfacial curvature and pressure difference was actually inadequate, and proposed more complicated formulations. He also concluded from his fourth-order theory that the growth rate of instability was less than that predicted by linear theory both with and without interfacial tension.

The stability theories of Chuoke et al. [12] and Outmans [13] were for waterfloods in parallel plate models which may differ from floods in a real porous medium or, for that matter, in a packed laboratory model. Benham and Olson [14] undertook a study to identify the important factors, including packing of a model, affecting viscous fingering in a laboratory model. The displacing and displaced fluids were of the same density to avoid gravity effects. They found that fingering was more severe in a packed model than in a Hele-Shaw model for the same mobility ratio, indicating that packing was an important variable in the fingering phenomena. It was also observed that the frontal distortion varied linearly with the distance displaced. Increased mobility ratio resulted in an increase in frontal distortion. Displacement velocity also had the same effect on the growth of fingers for both the packed and Hele-Shaw cells.

Similar conclusions were arrived at by Perkins and Johnston [15] in a later study. They studied immiscible fingering in linear Hele-Shaw and bead-packed models, the latter with, and without, an initial water saturation. Displacements were performed at both favourable and unfavourable viscosity ratios. It was found that Hele-Shaw displacements were inadequate for modelling the mechanism of immiscible fingering in a reservoir. They observed that the presence of a connate-water saturation had a significant influence on the displacement behaviour in a bead-packed model, especially when the viscosity ratio was unfavourable. Hence, they concluded that experiments aimed at studying immiscible fingering in water-wet porous media should

be conducted with a residual connate-water saturation. In the bead-packed models, they observed flat, piston-like displacement fronts at favourable mobility ratios. At unfavourable mobility ratios, numerous small fingers developed and the recovery efficiency at water breakthrough was significantly less than that for the favourable mobility ratio displacement. They observed that at unfavourable viscosity ratios, viscous fingers formed earlier during displacements with high injection rates. It was observed also that the shape of particles constituting the porous medium had only a slight influence on the recovery efficiency.

Like Perkins and Johnston [15], Gupta and co-workers conducted experiments to investigate viscous fingering in a Hele-Shaw cell [16] and also in a porous medium packed with glass beads [17]. It was found that after the incipient fingers formed, they degenerated to one finger which dominated the subsequent part of the displacement process. In the experiments conducted in the homogeneous Hele-Shaw model, the number of incipient fingers matched exactly that predicted by Chuoke's theory [12]. However, in the experiments in porous media, the displacement front was not sharp and the number of incipient fingers could not be counted. One very significant conclusion reached by the authors was that for all flow rates considered, the longitudinal finger growth was linear with time, both in the Hele-Shaw and the porous-medium models. Based on the experimental results obtained independently from these two studies, the authors concluded that the Hele-Shaw cell was indeed a valid tool for studying viscous fingering phenomena for a horizontal immiscible displacement process.

From the above-mentioned stability studies of immiscible displacement, it can be seen that the different variables, which are important from the point of view of immiscible interfacial instability, are viscosity ratio, capillary and gravitational forces, displacement rate and system permeability and wettability. However, none of the authors of these studies have been able to combine all of these variables into one

universal dimensionless group which can be used to quantify the stability boundary in a linear immiscible displacement. Peters and Flock [18] were the first authors who combined all of the variables pertinent to the stability problem into one dimensionless number which could be used to predict the onset of instability during linear immiscible displacements in cylindrical and rectangular systems. They extended the theory of Chuoke et al. [12] by imposing an additional boundary condition at the core wall where the perturbation velocity normal to the wall was made to vanish. This condition enabled them to incorporate the system dimensions into their stability analysis and also helped them to arrive at the critical value for the dimensionless number, beyond which the displacement would be unstable. Experiments were carried out in horizontal cylindrical cores and photographs of sections of the cores were taken under ultraviolet lighting. Measurement of the average dimensions of the fingers enabled them to estimate the "wettability numbers" for water-wet and oil-wet porous media, and thus the dimensionless number could be calculated. It was observed that beyond the stability boundary predicted by their theory [18], there was an initial rapid decrease in breakthrough recovery, with a tendency towards an eventual stabilization of recovery (pseudostable region) at a lower level than in the stable regime. Noteworthy in the analysis of Peters and Flock is the importance of the system dimensions which are raised to the power of two in the dimensionless stability numbers, while all other variables are raised to the power of one.

In their theory, Peters and Flock [18] used a sharp interface approximation and based their analysis on the concept of a velocity potential. While such an approach can deal with an incipient finger, it cannot deal with the subsequent growth of the finger [19]. Also, a velocity potential exists only for fields of flow involving a fluid of constant viscosity and density and a porous medium which is homogeneous and isotropic throughout [20,21]. Moreover, the approach of Peters and Flock was not able to account for the relative finger widths of the oil and water fingers.

In 1985, Bentsen [19], using the concept of a force potential, proposed a new approach to study the fingering phenomena. The approach taken was to define the force potential for the water on the oil side and on the water side of the interface, from which the perturbation potential for the water could be determined. This perturbation potential, when combined with the appropriate form of Darcy's law, would give the perturbation velocities for a water finger. A similar approach was followed to determine the perturbation velocities for an oil finger. The perturbation velocities for water and oil fingers were then combined by using several compatibility conditions, and the resulting system of equations was solved to obtain an expression for the eigenvalue dictating the width of a penetrating finger. Finally, by choosing an eigenvalue that dictated the largest wavelength that could fit within the confines of a rectangular porous medium, the instability number and its critical value were defined. Bentsen's theory [19] was able to account for the fact that water fingers were wider than the oil fingers and, thus, his instability number for a rectangular system was proportional to the one proposed by Peters and Flock [18] for the same system, the constant of proportionality being a function of mobility ratio.

In order to estimate one of the parameters in the defining equation for his instability number, the pseudointerfacial tension, Bentsen [22] suggested that the problem be approached at the macroscopic level rather than the microscopic level. By employing the concept of a force potential, he was able to derive a defining equation for the pseudointerfacial tension associated with a smooth, continuous pseudosurface located within a porous medium. Because the pseudointerfacial tension was defined in terms of the area under the capillary-pressure-versus-saturation curve, he defined a functional relationship for capillary pressure which can be used to estimate this area. Thus, if the area under the capillary-pressure curve, and hence the pseudointerfacial tension, need to be estimated, a capillary-pressure-versus-water-saturation relationship must be established through laboratory experiments for a particular rock-fluid system.

Recent experimental studies [23,24] have shown that the distance travelled by the tip of the water and oil fingers with respect to the moving boundary was not a non-linear time function as was assumed by Bentsen [19], but was in fact a linear function of time as was observed by Gupta et al. [16,17]. The experiments, conducted in Hele-Shaw cells, also confirmed the theoretical contention that water fingers are wider than oil fingers. The same conclusion regarding relative finger widths was obtained by Coskuner and Bentsen [25] when they modified Bentsen's earlier theory [19] to include a linear time function. Their modified theory was able to predict the stability boundary for Hele-Shaw displacements correctly. However, the predicted perturbation velocity in their theory was significantly higher than the measured perturbation velocity. The major reason for this discrepancy between measured and predicted perturbation velocities could be the loss of flow details near the nose of the finger, such loss having come about because of averaging of the flow information in the transverse direction to flow. The averaging was undertaken in order to establish an analogy between two-dimensional flow in a porous medium and flow in a Hele-Shaw cell.

Very good agreement between theory and experiment was attained in a study undertaken by Sarma and Bentsen [26]. Their three-dimensional theory, a modified version of Bentsen's stability theory [19] developed for flow through porous media, was successfully applied to predict the perturbation velocity of viscous fingers in a linear, rectangular-shaped, unconsolidated porous medium. Experimental results demonstrated that the modified theory of Sarma and Bentsen was able to predict not only the stability boundary for immiscible displacement in a rectangular core, but also the breakthrough recoveries for stable and pseudostable displacements.

3. STATEMENT OF THE PROBLEM

From the survey of the literature in the preceding section, two major observations can be made. First, it is clear that immiscible displacement of two fluids in a porous medium is either stable or unstable, depending on whether the combination of capillary and gravitational forces exceeds the viscous force, or vice versa. The stability of an immiscible displacement process is an important factor controlling the displacement efficiency. This emphasizes the importance of stability analysis to predict the onset of instability during a displacement process.

The second important observation is that linear stability theories, based either on the Buckley-Leverett model [1-4] or on the moving-boundary model with a velocity-potential approach [12,18], have some significant problems. In order to overcome these limitations, Bentsen [19] developed a stability analysis, based on the concept of a force potential, for immiscible displacements in a rectangular system.

However, most laboratory studies of linear displacements are carried out in cylindrical, and not in rectangular, sand packs. Thus, there is a need to develop a stability theory for immiscible displacement of two fluids for a cylindrical porous medium. In particular, the theory should be able to describe the entire life span of the viscous finger. Also, this theory should be able to account for the relative finger widths of the oil and water fingers and should be simple enough to have an analytical solution.

Thus, the purpose of this study is to develop a stability theory for immiscible displacement in a cylindrical system by utilizing a force-potential approach. The theory should be able to predict not only the stability boundary, but also the breakthrough recoveries for stable and pseudostable displacements. Subsequently, the theory is to be validated experimentally.

A further aim of this study is to perform a statistical error (sensitivity) analysis on the calculations of the instability number and the breakthrough recoveries for stable

and pseudostable displacements for a cylindrical system. The objective of the error analysis is to determine the relative contributions of both the variability due to measurement of the relevant variables, and the variability due to the sand properties and the packing procedure to the total standard deviations of the instability number and the breakthrough recovery.

4. DEVELOPMENT OF STABILITY THEORY

4.1 Introduction

The success of most secondary-recovery schemes may depend upon whether the displacement is stable or unstable. Thus, the identification of the stability boundaries during such displacements is of interest. For this purpose, stability theories have been developed for immiscible displacements in rectangular systems [19, 26]. However, most laboratory displacement experiments are carried out in cylindrical, and not rectangular, cores. The purpose of this section is to demonstrate the development of a stability theory for cylindrical systems.

The theory presented here is based on the assumption that the oil-water immiscible displacement process can be treated as a moving boundary problem. Thus, in order to study the behaviour of a perturbation of the interface separating the two fluids, the potential on each side of the interface must be specified. Such potentials arise out of the contribution of capillary, gravitational and viscous forces. The contribution of gravitational and viscous forces can be readily quantified [19, 26]. However, in order to estimate the contribution of the capillary forces, it is necessary to know how the boundary ξ, which separates the displaced fluid from the displacing fluid, evolves as the amplitude of the surface increases in magnitude with time.

The mathematical prediction of the evolution of the surface separating the two fluids presents problems. The first reason for this is that the two fluids, in reality, are separated by a transition zone (capillary fringe) and not by a plane interface. However, it has been suggested in previous studies [19, 26, 27] that, when the capillary forces are significant, the transition zone is relatively small when compared to the diameter of the sandpack. This suggests that it may be possible, without introducing significant error, to replace the transition zone by a sharp, plane macroscopic interface to which pressure discontinuities are assigned, and up to which the relatively uniform saturation and flow conditions prevailing outside the transition zone are extrapolated. The second

problem associated with the theoretical prediction of the evolution of the pseudosurface is that the potential distribution on each side of the interface is a function of the location of the surface. This means that the potential distributions must be determined simultaneously with ξ, which creates great difficulties. In order to deal with this problem, it is assumed that the potentials may be specified a priori. Then, it is possible to develop the partial differential equation describing the evolution of the two-dimensional pseudosurface separating the water from the oil. This equation may be derived by undertaking a summation of the normal forces acting on a differential element of the pseudosurface. The solution to this equation is used to determine the contribution of the capillary forces to the potential distribution.

Once the force potentials for the water on the water side and on the oil side of the interface are specified, the perturbation potential for the water can be determined from the difference between these two potentials. From the equation for the perturbation potential for the water, expressions for the water perturbation velocities are obtained by the use of the appropriate form of Darcy's law. A similar approach is used to determine the perturbation velocities for an oil finger. Finally, by application of appropriate boundary conditions and several compatibility conditions to the perturbation velocities for the oil and water fingers, an expression for the dimensionless instability number is determined. Also, its critical value is obtained, beyond which the displacement becomes unstable. The details of this approach are presented in the following sections.

4.2 Capillary Pressure Potential

To determine the capillary pressure potential, one must know how the boundary ξ, which separates the displacing fluid from the displaced fluid, evolves spatially and temporally. Assuming that the force potentials on either side of the interface may be specified a priori, the two-dimensional pseudosurface separating the two fluids can be

described by means of a partial differential equation, which is obtained by undertaking a summation of the normal forces acting on a differential element of the surface. The differential equation describing the evolution of such a pseudosurface, in rectangular systems has been shown to be [26, 27]

$$\sigma_e\left[\frac{\partial^2(\xi_w)_o}{\partial x^2} + \frac{\partial^2(\xi_w)_o}{\partial y^2}\right] + \left(P_{cw}(x, y, z)\right)_0 = 0 \qquad (1)$$

where $(\xi_w(x, y, z))_0$ gives the displacement of any point on the surface as a function of the spatial coordinates and $(P_{cw}(x, y, z))_0$ is the pressure difference across the interface. The pseudointerfacial tension, σ_e, is assumed to be uniform over the pseudosurface. The equivalent equation in the cylindrical coordinate system is [28]

$$\sigma_e\left[\frac{\partial^2(\xi_w)_o}{\partial r^2} + \frac{1}{r}\frac{\partial(\xi_w)_o}{\partial r} + \frac{1}{r^2}\frac{\partial^2(\xi_w)_o}{\partial \theta^2}\right] + \left(P_{cw}(r, \theta, z)\right)_0 = 0 \qquad (2)$$

Equation 2 can be derived also independently to describe the evolution of the pseudosurface separating the oil from the water in cylindrical systems [see Appendix A]. It is to be noted that only the positive domain of the solution to the above equation is used in the subsequent analysis.

4.3 Macroscopic Capillary Pressure

In order to define the macroscopic capillary pressure, $(P_{cw})_o$, the water perturbation potential, $(\Phi_w^*)_o$, must be specified. The water perturbation potential in the region where the oil is flowing is defined by [19]

$$\left(\Phi_w^*\right)_o = \frac{\Delta\rho}{\rho_w} gz \cos\alpha + \frac{\rho_o}{\rho_w}\left(\Phi_o\right)_o - \left(\Phi_w\right)_w + \frac{\left(P_{cw}\right)_o}{\rho_w} + \frac{P_c(t)}{\rho_w} \tag{3}$$

where $(\Phi_w)_w$ and $(\Phi_o)_o$ are defined, respectively, by

$$\vec{v}_w = -\frac{k_{wor}\,\rho_w}{\mu_w}\nabla\left(\Phi_w\right)_w \tag{4}$$

and

$$\vec{v}_o = -\frac{k_{oiw}\,\rho_o}{\mu_o}\nabla\left(\Phi_o\right)_o \tag{5}$$

Now, assuming that, on the interface, $v_{wz} = v_{oz} = v$, and that, k_{wor} and k_{oiw} are independent of z, it may be shown by integrating Equations 4 and 5, respectively, that

$$\left(\Phi_w\right)_w = \Phi_{wi} - \frac{\mu_w\, v}{k_{wor}\,\rho_w}\left(\xi_w\right)_o \tag{6}$$

and

$$\left(\Phi_o\right)_o = \Phi_{oi} - \frac{\mu_o\, v}{k_{oiw}\,\rho_o}\left(\xi_w\right)_o \tag{7}$$

where Φ_{wi} is the initial value of the potential in the water in the region where water is flowing and Φ_{oi} is the initial value of the potential in the oil in the region where oil is flowing.

If the expressions for $(\Phi_w)_w$ and $(\Phi_o)_o$, from Equations 6 and 7, respectively, are introduced into Equation 3, we get, after some manipulation,

$$\left(\Phi_w^*\right)_o = -\frac{1}{\rho_w}\left[\frac{\mu_w v}{k_{wor}}(M-1-N_g)\left(\xi_w\right)_o-(P_{cw})_o\right] + \frac{1}{\rho_w}\left[\rho_o \Phi_{oi} - \rho_w \Phi_{wi} + P_c(t)\right] \quad (8)$$

where

$$M = \frac{k_{wor}\,\mu_o}{k_{oiw}\,\mu_w} \quad (9)$$

and

$$N_g = \frac{\Delta\rho\; g\; k_{wor}\; \text{Cos}\;\alpha}{\mu_w\; v} \quad (10)$$

At zero displacement of the interface, the surface is plane. If it is assumed that $(P_{cw})_o$ is zero at zero displacement of the interface, then it can be shown from Equation 8, that

$$\left(\Phi_w^*(z=0)\right)_o = \frac{1}{\rho_w}\left[\rho_o \Phi_{oi} - \rho_w \Phi_{wi} + P_c(t)\right] \quad (11)$$

Again, if the roots of the viscous fingers are to remain fixed in the surface which initially separates the two flowing fluids, it is necessary that $(\Phi_w^*(z=0))_o$ be zero [26]. In that case, we have, from Equation 11

$$P_c(t) = -(\rho_o \Phi_{oi} - \rho_w \Phi_{wi}) \quad (12)$$

That is, $P_c(t)$ turns out to be the pressure difference which existed across the pseudosurface, prior to its being perturbed.

Combining Equations 8 and 12, we get

$$\rho_w (\Phi_w^*)_o = -\frac{\mu_w v}{k_{wor}}(M-1-N_g)\,(\xi_w)_o + (P_{cw})_o \quad (13)$$

Equation 13 defines the pressure difference across the pseudosurface corresponding to a given perturbation of the surface, $(\xi_w)_o$. If the normal forces acting on the surface were in equilibrium, the perturbation potential would be zero, and the equilibrium pressure difference across the interface would be defined by

$$(P_{cw})_{oe} = \frac{\mu_w v}{k_{wor}} (M - 1 - N_g) (\xi_w)_o \tag{14}$$

However, when a viscous finger starts propagating, the forces acting on the surface will not be in equilibrium. In that situation, the pressure difference across the interface will be slightly smaller than the equilibrium macroscopic capillary pressure, $(P_{cw})_{oe}$ [26]. Assuming that the actual capillary pressure is proportional to $(P_{cw})_{oc}$, the macroscopic capillary pressure can be defined by

$$(P_{cw})_o = \frac{\beta_w (M) \mu_w v}{k_{wor}} (M - 1 - N_g) (\xi_w)_o \tag{15}$$

where β_w (M), the constant of proportionality, is a function of M (see Equation 74). The nature of the dependence of β_w (M) on M, as will be seen later, also depends on the core geometry.

4.4 Equation for Pseudosurface

Introducing the definition of the macroscopic capillary pressure from Equation 15 into Equation 2, we have

$$\frac{\partial^2 (\xi_w)_o}{\partial r^2} + \frac{1}{r} \frac{\partial (\xi_w)_o}{\partial r} + \frac{1}{r^2} \frac{\partial^2 (\xi_w)_o}{\partial \theta^2} + \frac{\beta_w (M) \mu_w v}{k_{wor} \sigma_e} (M - 1 - N_g) (\xi_w)_o = 0 \tag{16}$$

Then, defining

$$\gamma_w^2 = \frac{\beta_w (M)\, \mu_w\, v}{k_{wor}\, \sigma_c} (M - 1 - N_g) \tag{17}$$

it follows that

$$\frac{\partial^2 (\xi_w)_o}{\partial r^2} + \frac{1}{r} \frac{\partial (\xi_w)_o}{\partial r} + \frac{1}{r^2} \frac{\partial^2 (\xi_w)_o}{\partial \theta^2} + \gamma_w^2 (\xi_w)_o = 0 \tag{18}$$

The solution to Equation 18, by the method of separation of variables [29, 30], can be obtained as follows. Let

$$(\xi_w)_o = R(r) \cdot \Theta(\theta) \tag{19}$$

That is to say, we assume that $(\xi_w)_o$, which is a function of r and θ, is the product of a funtion of r and a function of θ. Both the functions R and Θ are real-valued. Introducing Equation 19 into Equation 18, we have

$$R'' \Theta + \frac{1}{r} R' \Theta + \frac{1}{r^2} R \Theta'' + \gamma_w^2 R \Theta = 0 \tag{20}$$

When Equation 20 is divided on both sides by $\frac{R\Theta}{r^2}$, it can be written as

$$-\left[\frac{r^2 R'' + rR'}{R} + \gamma_w^2 r^2\right] = \frac{\Theta''}{\Theta} \tag{21}$$

Now, when a function of one variable equals a function of another variable, the two functions must be equal to the same constant, which is a negative number [31]. Thus, we get

$$-\left[\frac{r^2 R'' + rR'}{R} + \gamma_w^2 r^2\right] = -\mu^2 = \frac{\Theta''}{\Theta} \tag{22}$$

where μ is an integer. Breaking Equation 22 up into two different equations, each involving functions of one fundamental variable, we get

$$\Theta'' + \mu^2 \Theta = 0, \quad -\pi < 0 < \pi \tag{23}$$

and

$$r^2 R'' + rR' + \left(\gamma_w^2 r^2 - \mu^2\right) R = 0, \quad 0 < r < a \tag{24}$$

Now, upon introducing the conditions

$$\Theta(-\pi) = \Theta(\pi) \tag{25}$$

and

$$\Theta'(-\pi) = \Theta'(\pi) \tag{26}$$

we have, by solving Equation 23 [32]

$$\Theta(\theta) = C \operatorname{Cos} n\theta \tag{27}$$

where C is the constant of proportionality and n = 1, 2, 3, ... Again, the general solution to Equation 24 is [33]

$$R(r) = C_1 J_n(\gamma_w r) + C_2 Y_n(\gamma_w r) \tag{28}$$

where C_1 and C_2 are constant. The funtion $J_n (\gamma_w r)$ is called Bessel's function of order n and $Y_n (\gamma_w r)$ is called Neumann's Bessel function of the second kind of order n. Now, as r tends to zero, Y_n tends to infinity. But, in the present problem, the singular Bessel function cannot be used, because we want a solution that is regular at the origin. Thus, in order that R (r) be bounded, C_2 must be zero. Therefore, Equation 28 yields

$$R(r) = C_1 J_n (\gamma_w r) \tag{29}$$

Again, since any multiple of a solution is another solution [34], we can drop the constant C_1 in Equation 29 and the constant C in Equation 27, and by combining them, we get from Equation 19

$$(\xi_w)_o = Z_w J_n (\gamma_w r) \cos n\theta \tag{30}$$

where Z_w, the amplitude of a water finger, is a linear function of time [17, 24, 26] (see Equation 45).

4.5 Perturbation Velocities

Introducing Equation 17 into Equation 15, the macroscopic capillary pressure in the region where the oil is flowing may be defined by

$$(P_{cw})_o = \sigma_e \gamma_w^2 (\xi_w)_o \tag{31}$$

A similar approach may be taken to show that the macroscopic capillary pressure in the region where water is flowing may be defined by

$$(P_{co})_w = \sigma_e \gamma_o^2 (\xi_o)_w \tag{32}$$

By combining the appropriate forms of Darcy's law with Equations 31 and 32, it can be shown that the perturbation velocities in the radial direction in the region where the oil is flowing and in the region where the water is flowing, respectively, are

$$\left(v^*_{wr}\right)_o = -\frac{k_{w\alpha r}}{\mu_w}\,\sigma_e\gamma_w^2\,\frac{\partial\left(\xi_w\right)_o}{\partial r} \tag{33}$$

and

$$\left(v^*_{\alpha r}\right)_w = -\frac{1}{M}\,\frac{k_{w\alpha r}}{\mu_w}\,\sigma_e\gamma_o^2\,\frac{\partial\left(\xi_o\right)_w}{\partial r} \tag{34}$$

The perturbation velocities in the z-direction, in the region where the oil is flowing and in the region where the water is flowing, respectively, can be shown to be [26, 27]

$$\left(v^*_{wz}\right)_o = \left[v\left(M-1-N_g\right) - \frac{k_{w\alpha r}}{\mu_w}\,\sigma_e\gamma_w^2\right]\frac{\partial\left(\xi_w\right)_o}{\partial z} \tag{35}$$

and

$$\left(v^*_{\alpha z}\right)_w = -\frac{1}{M}\left[v\left(M-1-N_g\right) - \frac{k_{w\alpha r}}{\mu_w}\,\sigma_e\gamma_o^2\right]\frac{\partial\left(\xi_o\right)_w}{\partial z} \tag{36}$$

4.6 Time Function

While Equation 30 indicates how $(\xi_w)_o$ depends on r, θ and z_w, it does not show how z_w depends on t. To derive the nature of the dependence of z_w on t, it can be shown, by using Equations 33, 34, 35 and 36, that [26, 27]

$$(v^*_{wr})_o = \frac{\partial(\xi_w)_o}{\partial r} \cdot \frac{dr}{dt} = -\frac{k_{wo}}{\mu_w} \sigma_e \gamma_w^2 \frac{\partial(\xi_w)_o}{\partial r} \tag{37}$$

$$(v^*_{or})_w = \frac{\partial(\xi_o)_w}{\partial r} \cdot \frac{dr}{dt} = -\frac{1}{M} \frac{k_{wo}}{\mu_w} \sigma_e \gamma_o^2 \frac{\partial(\xi_o)_w}{\partial r} \tag{38}$$

$$(v^*_{wz})_o = \frac{\partial(\xi_w)_o}{\partial z} \cdot \frac{dz}{dt} = \left[v(M - 1 - N_g) - \frac{k_{wo}}{\mu_w} \sigma_e \gamma_w^2\right] \frac{\partial(\xi_w)_o}{\partial z} \tag{39}$$

and

$$(v^*_{oz})_w = \frac{\partial(\xi_o)_w}{\partial z} \cdot \frac{dz}{dt} = -\frac{1}{M}\left[v(M - 1 - N_g) - \frac{k_{wo}}{\mu_w} \sigma_e \gamma_o^2\right] \frac{\partial(\xi_o)_w}{\partial z} \tag{40}$$

From Equations 37, 38, 39 and 40, it can be seen that

$$\frac{dr_w}{dt} = \frac{k_{wor}}{\mu_w} \sigma_e \gamma_w^2 \tag{41}$$

$$\frac{dr_o}{dt} = -\frac{1}{M} \frac{k_{wor}}{\mu_m} \sigma_e \gamma_o^2 \tag{42}$$

$$\frac{dz_w}{dt} = \left[v(M - 1 - N_g) - \frac{k_{wo}}{\mu_w} \sigma_e \gamma_w^2\right] \tag{43}$$

and

$$\frac{dz_o}{dt} = -\frac{1}{M}\left[v(M - 1 - N_g) - \frac{k_{wo}}{\mu_w} \sigma_e \gamma_o^2\right] \tag{44}$$

Equations 41 and 42 define the rates of radial increase of the bases of a water finger and an oil finger, respectively. Equations 43 and 44 define the rates of increase

of the amplitudes, in the z-direction, of a water finger and an oil finger, respectively. These equations have been developed with the assumption that the roots of the water and oil fingers remain attached to the surface which initially separated the water from the oil.

From Equation 43, it can be seen that the velocity of propagation of a water finger remains the same for any given value of γ_w, provided the superficial velocity of displacement, v, remains constant. Thus, it can be written that

$$z_w = z = a_w + (v^*_{wm})_o \, t \tag{45}$$

where a_w is the initial amplitude of the water finger and where $(v^*_{wm})_o$ is defined by Equation 43. Similarly, for an oil finger, it can be seen from Equation 44 that

$$z_o = -z = -a_o - (v^*_{om})_w \, t \tag{46}$$

where a_o is the initial amplitude of an oil finger, and where $(v^*_{om})_w$ is defined by Equation 44.

Introducing Equation 45 into Equation 30 yields, for the surface of a water finger in the region where oil is flowing,

$$\left(\eta_w(r, \theta, t)\right)_o = J_n(\gamma_w r) \operatorname{Cos} n\theta \left\{a_w + (v^*_{wm})_o \, t\right\} \tag{47}$$

Differentiating Equation 47 with respect to t yields the expression for the rate of increase of the amplitude of the finger surface,

$$\frac{\partial (\eta_w)_o}{\partial t} = (v^*_{wm})_o \; J_n(\gamma_w r) \operatorname{Cos} n\theta \tag{48}$$

4.7 Minimum Geometric Eigenvalue

The radial perturbation velocity of a water finger, $(v^*_{wr})_o$, is proportional to $\frac{\partial(\eta_w)_o}{\partial r}$. Two conditions are applied to the radial peturbation velocity, in order to model a water finger. First, the velocity normal to the core wall must vanish [18, 32]; that is, $(v^*_{wr})_o$ must be zero at r = a, where a is the core radius. Applying this boundary condition, it may be shown that

$$J'_n (\gamma_w a) = 0 \tag{49}$$

The second condition is that the radial perturbation velocity of a water finger is not zero at the centre of the core. That is to say, J'_n (0) should not equal zero. Based on these two conditions, it can be concluded that n = 1, so that Equation 47 becomes

$$\eta_w (r, \theta, t) = J_1(\gamma_w r) \cos \theta \left\{a_w + (v^*_{wm})_o t\right\} \tag{50}$$

where J_1 is Bessel function of the first order.

For any particular value of n, Equation 49 has an infinite number of possible roots, α_m, where m is the mode number. Table 1, taken from Reference 35, lists the first few positive roots of J_n and J'_n, for different values of n. The roots of J'_n listed under any particular value of n, being the product of the wavenumber and the core radius, give a qualitative indication of the possible wavelengths of the fingers [18]. Thus, for n = 1, and for fingering to take place, the value of $(\gamma_w a)$ has to be at least equal to 1.8412, the first mode value. Therefore, the minimum geometric eigenvalue is given by

Table 1: Zeros of Bessel Functions $J_n(x)$ and $J_n'(x)$*

	n = 0	n = 1	n = 2	n = 3
$J_n(x) = 0$	2.4048	3.8317	5.1356	6.3802
	5.5201	7.0156	8.4172	9.7610
	8.6537	10.1735	11.6198	13.0152
	11.7915	13.3237	14.7960	16.2235
$J_n'(x) = 0$	0.0000	1.8412	3.0542	4.2012
	3.8317	5.3314	6.7061	8.1052
	7.0156	8.5363	9.9695	11.3459
	10.1735	11.7060	13.1704	14.5859

* from Reference 35

$$\gamma_{w_{geom.}} = \frac{1.8412}{a} \tag{51}$$

which shows that

$$\gamma^2_{w_{geom.}} = \frac{3.39}{a^2} \tag{52}$$

4.8 Compatibility Conditions

Certain conditions must be met if the growth of two or more pairs of oppositely directed oil and water fingers is to be compatible. The conditions of symmetry, continuity and similarity, which have been applied before in rectangular systems [19], are also imposed here in order to ensure the compatibility of the growth of the fingers.

The functional forms are the same for both the oil and the water fingers. Consequently, for the condition of symmetry to be met, the roots of the oil and water fingers must be located symmetrically within the circular interface which initially separated the oil from the water. This condition can be imposed by making the integral values of the mode numbers for the oil and the water fingers equal. The condition of similarity requires that the shape of a given water finger be similar to that of the contiguous oil finger over the entire time span of finger growth. Similarity can be guaranteed by requiring that the ratio of the velocities of a water finger and the adjacent oil finger be the same in all directions. The condition of continuity can be met by requiring that the volume of water contained within a water finger be the same as the volume of oil contained within the continguous, oppositely directed oil finger.

Now, it can be seen from Equations 39 and 40 that

$$(v^*_{wz})_o = \left[v\,(M - 1 - N_g) - \frac{k_{wo}}{\mu_w}\,\sigma_e \gamma_w^2\right] J_1(\gamma_w r)\,\mathrm{Cos}\,\theta \qquad (53)$$

and

$$(v^*_{oz})_w = -\frac{1}{M}\left[v\,(M - 1 - N_g) - \frac{k_{wo}}{\mu_w}\,\sigma_e \gamma_o^2\right] J_1(\gamma_o r)\,\mathrm{Cos}\,\theta \qquad (54)$$

At equivalent locations on the surface, the value of $\{J_1(\gamma r)\,\mathrm{Cos}\,\theta\}$ should be the same for both the oil and the water fingers. Therefore, at equivalent locations on the surface, it can be seen from Equations 53 and 54 that

$$\frac{(v^*_{wz})_o}{(v^*_{oz})_w} = \frac{(v^*_{wm})_o}{(v^*_{om})_w} \qquad (55)$$

Again, we have from Equations 37 and 38

$$(v^*_{wr})_o = -\frac{k_{wo}}{\mu_w}\,\sigma_e \gamma_w^3 \left\{a_w + (v^*_{wm})_o\, t\right\} J_1'(\gamma_w r)\,\mathrm{Cos}\,\theta \qquad (56)$$

and

$$(v^*_{or})_w = -\frac{1}{M}\,\frac{k_{wo}}{\mu_w}\,\sigma_e \gamma_o^3 \left\{a_o + (v^*_{om})_w\, t\right\} J_1'(\gamma_o r)\,\mathrm{Cos}\,\theta \qquad (57)$$

Using the same approach as before, it follows that at equivalent locations on the surface and at $t = 0$

$$\frac{(v^*_{wr})_o}{(v^*_{or})_w} = \frac{M\,\gamma_w^3\,a_w}{\gamma_o^3\,a_o} \tag{58}$$

For the condition of similarity to be true, it may be shown, from Equations 55 and 58, that

$$\frac{(v^*_{wm})_o}{(v^*_{om})_w} = \frac{M\,\gamma_w^3\,a_w}{\gamma_o^3\,a_o} \tag{59}$$

The volume of water contained within a water finger is defined by

$$V_w = \int_o^{\pi/2} \int_o^a \eta_w\,(r, \theta, t)\, r\, dr\, d\theta \tag{60}$$

Introducing Equation 50 into Equation 60, it can be shown, by considering only the first term of the expanded form of J_1, that an approximate value for the volume of a water finger is given by

$$V_w = \frac{[a_w + (v^*_{wm})_o\, t]}{6}\, \gamma_o\, a^3 \tag{61}$$

Similarly, the volume of oil contained within an oil finger can be shown to be

$$V_o = \frac{[a_o + (v^*_{om})_w\, t]}{6}\, \gamma_o\, a^3 \tag{62}$$

Equations 61 and 62 can also be arrived at by using Kronecker's formula [26], and by considering the first two terms of the expanded form of J_0 For the condition of

continuity to be true, V_w should be equal to V_o and the relationship obtained thereby should hold true even when t = 0. Applying this condition, it may be shown that

$$\frac{a_w}{a_o} = \frac{\gamma_o}{\gamma_w} \tag{63}$$

Now, Equations 45 and 46 yield

$$a_w = z_w - (v^*_{wm})_o\, t \tag{64}$$

and

$$a_o = z_o - (v^*_{om})_o\, t \tag{65}$$

from which, it can be seen, at t = 0, that

$$\frac{a_w}{a_o} = \frac{z_w}{z_o} \tag{66}$$

so that, it follows that

$$\frac{a_w}{a_o} = \frac{z_w}{z_o} = \frac{(v^*_{wm})_o}{(v^*_{om})_w} \tag{67}$$

Combining Equations 59 and 67, it may be demonstrated that

$$\gamma_o^3 = M\,\gamma_w^3 \tag{68}$$

which implies that the wavelength of a water finger is $M^{1/3}$ times that of the contiguous oil finger. The validity of this relationship has been confirmed experimentally in analogue models of porous media [23, 24], and has also been confirmed indirectly in previous studies for rectangular systems [19, 26, 27]. Also, introducing Equation 68 into Equation 63, it can be shown that

$$a_w = M^{1/3} a_o \tag{69}$$

which relates the initial amplitudes of disturbance for oil and water fingers, by means of a function of the mobility ratio. It is to be noted that Equations 68 and 69 can also be derived by considering all the terms of the expanded form of J_1.

4.9 Velocity of Penetrating Fingers

The four unknowns $(v^*_{wm})_o$, $(v^*_{om})_w$, γ_w and γ_o are related by the four equations: 43, 44, 68 and 70, where Equation 70, which is given as

$$\frac{(v^*_{wm})_o}{(v^*_{om})_w} = \frac{\gamma_o}{\gamma_w} = M^{1/3} \tag{70}$$

relates the maximal propagation rates of the water and the oil fingers. Equations 43, 44, 68 and 70 may be solved to arrive at an expression for the maximal velocity of the penetrating water finger, as

$$(v^*_{wm})_o = \frac{v\,(M - 1 - N_g)}{2} \left(\frac{M^{2/3} - 1}{M^{2/3}} \right) \tag{71}$$

Also, by combining Equations 70 and 71, it can be demonstrated that the maximal velocity of the penetrating oil finger is given by

$$(v^*_{om})_w = \frac{v(M-1-N_g)}{2}\left(\frac{M^{2/3}-1}{M}\right) \tag{72}$$

4.10 Eigenvalue for the Water Region

Comparing the two defining Equations for $(v^*_{wm})_o$, 43 and 71, it may be shown that

$$\gamma_w^2 = \frac{\mu_w v(M-1-N_g)}{k_{wo}\sigma_e}\left(\frac{M^{2/3}+1}{2M^{2/3}}\right) \tag{73}$$

where γ_w is the eigenvalue for the water region and it corresponds to a particular superficial velocity, v. A comparison of Equation 73 with Equation 17 reveals that β_w (M) is defined by

$$\beta_w(M) = \frac{M^{2/3}+1}{2M^{2/3}} \tag{74}$$

It should be noted that β_w (1) equals one and β_w (∞) equals 0.5, and for values of M between one and infinity, β_w (M) gradually changes from 0.5 to one, the amount depending on the value of M.

It should also be noted that, as distinguished from this case, the β_w (M) in the case of a rectangular system, has been defined by

$$\beta_w(M) = \frac{M^{5/3}+1}{(M+1)M^{2/3}} \tag{75}$$

4.11 Most Probable Finger Width

The ratio of the surface area to the volume of a water finger needs to be determined in order to develop the defining equation for the time constant of a water finger, from which the dominant wavelength of finger growth can be ascertained. The surface area of a water finger has been defined by [26]

$$A_{sw} = \int_o^{\pi/2} \int_o^{a} \sqrt{\left(\frac{\partial(\xi_w)_o}{\partial r}\right)^2 + \frac{1}{r^2}\left(\frac{\partial(\xi_w)_o}{\partial \theta}\right)^2}\; r\, dr\, d\theta \tag{76}$$

By introducing Equation 30 into Equation 76, and knowing that n = 1, and considering that only the first term of the expanded form of J_1 is used, an approximate value for the surface area of a water finger may be demonstrated to be

$$A_{sw} = \frac{\pi a^2}{8} \cdot z_w \gamma_w \tag{77}$$

In view of Equations 61 and 77, the surface-area-to-volume ratio of a water finger may be shown to be

$$\frac{A_{sw}}{V_w} = \frac{3\pi}{4a} \tag{78}$$

The time constant of a water finger is obtained by multiplying Equation 78 by the average velocity in the z-direction at which fluid is crossing the base of the finger [26]. The average velocity is obtained by integrating the peturbation velocity in the z-direction (given by Equation 53) over the total flow area. By undertaking this procedure, it can

be shown that the average rate at which water passes through the base of a water finger is related to the maximum velocity of the finger by

$$v_{wa} = (v^*_{wm})_o \cdot \gamma_w \cdot \frac{2a}{3\pi} \tag{79}$$

Hence, by combining Equations 43, 78 and 79, it can be demonstrated that the time constant of a water finger is defined by

$$n_w = \frac{\gamma_w}{2}\left[v(M-1-N_g) - \frac{k_{wo}}{\mu_w}\sigma_e\gamma_w^2\right] \tag{80}$$

The time constant n_w, which is associated with every finger wavelength, determines how fast each wavelength will grow for a given superficial velocity, v. The eigenvalue corresponding to zero growth rate for a finger is called the critical eigenvalue, and is found, by equating Equation 80 to zero and solving for the eigenvalue, to be

$$\gamma_c = \sqrt{\frac{\mu_w v(M-1-N_g)}{k_{wo}\sigma_e}} \tag{81}$$

Equation 81 defines the eigenvalue at which the perturbation velocity is zero. That is, γ_c is the eigenvalue at which the viscous forces exactly balance the capillary and gravitational forces.

It can be seen from Equation 81 that, with increasing velocity, fingers are formed with progressively smaller wavelengths. Among the wavelengths, the one that dominates the displacement has the maximum surface-creation rate per unit area [19, 23, 26]. In other words, the most probable finger is the one for which the time constant, as defined by Equation 80, is a maximum. Therefore, by differentiating

Equation 80 with respect to γ_w, and setting the resulting equation to zero, the dominant finger wavelength may be shown to be

$$\gamma_m^2 = \frac{1}{3}\gamma_c^2 \tag{82}$$

where γ_c is given by Equation 81. The above relationship has also been derived in many previous studies [12, 18, 19, 23, 26].

4.12 Stability Criterion

The type of displacement that takes place within the confines of a porous medium depends upon the balance existing among the viscous, capillary and gravitational forces. If the combined forces of gravity and capillarity are greater than the viscous forces, the displacement is stable. Otherwise, the displacement is unstable.

The effects of the viscous, capillary and gravitational forces on the wavelength of the viscous fingers is reflected in Equation 73. Equation 73 shows that for every velocity of displacement there is an associated wavelength of disturbance. However, because the displacement takes place within the confines of a porous medium, only those wavelengths which are smaller than a certain critical wavelength which is determined by the dimensions of the porous medium, may be manifested. Therefore, the largest wavelength which can fit within the confines of the porous medium determines the onset of instability [18, 19, 23, 26]. This largest wavelength corresponds to the smallest eigenvalue which is given by Equation 51.

Thus, for the displacement to be stable, it is required that

$$\gamma_w^2 \leq \gamma_{w\,geom}^2 \tag{83}$$

Introducing Equations 52 and 73 into Equation 83, it can be shown that the displacement is stable provided that

$$I_{sc} = \frac{\mu_w v (M - 1 - N_g) D^2}{k_{wo} \sigma_e} \left(\frac{M^{2/3} + 1}{2 M^{2/3}} \right) \leq 13.56 \tag{84}$$

It should be noted that the instability number for cylindrical systems defined by Equation 84 is proportional to the one developed by Peters and Flock [18], the constant of proportionality

$$C_c(M) = \frac{M^{2/3} + 1}{2M^{2/3}} \tag{85}$$

being a function of mobility ratio. This factor arises because proper account was taken, in the theory, of the fact that water fingers are wider than oil fingers [19]. The correction factor in the instability number for rectangular systems has been shown to be given by [19]

$$C_r(M) = \frac{4 (M^{5/3} + 1)}{(M + 1) (M^{1/3} + 1)^2} \tag{86}$$

4.12.1 Pseudointerfacial Tension

In order to determine the instability number for a displacement process using Equation 84, the pseudointerfacial tension, σ_e, must be estimated. In this study σ_e is estimated by making use of a recently developed mechanistic model [22] that requires the capillary-pressure-versus-saturation data for the rock-fluid system under consideration. This model for σ_e has also been used in some of the previous studies on

instability in rectangular systems [26, 27]. The parameter σ_c is calculated, by using the capillary-pressure-versus-saturation data, from

$$\sigma_c = \frac{A_c \, \emptyset \, (1 - S_{wi} - S_{or})}{1} \tag{87}$$

where A_c is the area under the capillary-pressure-versus-saturation curve.

4.13 Breakthrough Recovery

The breakthrough recovery of a displacement process can be estimated by using the equation for the perturbation velocity of a water finger (Equation 71) [19, 26]. However, certain assumptions have to made before deriving the equation for the breakthrough recovery. Also, these assumptions depend upon whether the displacement is stable or pseudostable.

4.13.1 Stable Displacements

The instability theory is based on the assumption that the displaced and displacing fluids are separated by a sharp displacement front, if the displacement is stable. However, in a real porous medium the two regions where only one fluid is flowing is not separated by a saturation discontinuity, but by a saturation transition region. To model this saturation distribution, it is assumed that the mobility ratio and the displacement velocity are such that the stability boundary has just been crossed (i.e., m = 1) and that, as a consequence, half of a water finger is propagating. The actual velocity of such a finger is obtained by adding the superficial velocity, v, to $(v^*_{wm})_o$ and then dividing by the porosity times the change in saturation [26]. The resulting equation may be shown to be

$$v_{wfa} = \frac{v}{\phi(1 - S_{wi} - S_{or})} \left[1 + \frac{M - 1 - N_g}{2} \cdot \frac{M^{2/3} - 1}{M^{2/3}} \right] \tag{88}$$

Now, let t_o be the time when fingering commences and t be the time, after fingering starts, when the tip of the finger reaches the outlet end of the core. Then, t_o is given by

$$t_o = \frac{Z_o A \varnothing (1 - S_{wi} - S_{or})}{Q} \tag{89}$$

and t by

$$t = \frac{(L - Z_o) A \phi (1 - S_{wi} - S_{or})}{Q\left[1 + \frac{M - 1 - N_g}{2} \cdot \frac{M^{2/3} - 1}{M^{2/3}}\right]} \tag{90}$$

where Q is the volumetric injection rate, Z_o is the location, along the length of the core, where fingering starts, and L is the core length. The total volumetric recovery at breakthrough is given by

$$R_t = q(t_o + t) = A \phi (1 - S_{wi} - S_{or})\left[Z_o + \frac{L - Z_o}{1 + \frac{M - 1 - N_g}{2} \cdot \frac{M^{2/3} - 1}{M^{2/3}}}\right] \tag{91}$$

Thus, the breakthrough recovery, as a fraction of the initial oil in place (IOIP), may be shown to be

$$R_{bt} = \frac{1 - S_{wi} - S_{or}}{1 - S_{wi}} \left[\frac{Z_o}{L} + \frac{1 - Z_o/L}{1 + \frac{M - 1 - N_g}{2} \cdot \frac{M^{2/3} - 1}{M^{2/3}}}\right] \tag{92}$$

Assuming that the fingering starts at the inlet end of the core, Equation 92 can be written as

$$R_{bt} = \frac{1 - S_{wi} - S_{or}}{1 - S_{wi}} \left[\frac{1}{1 + \frac{M - 1 - N_g}{2} \cdot \frac{M^{2/3} - 1}{M^{2/3}}} \right] \tag{93}$$

4.13.2 Pseudostable Displacements

For values of I_{sc} at or near 13.56, only one finger is propagating. However, as the instability number is increased above 13.56, increasing number of fingers with progressively smaller wavelengths can be formed. Which wavelength will dominate the displacement process depends upon the velocity of the displacement, and hence, the instability number I_{sc}. As the value of I_{sc} increases, the likelihood that the most probable wavelength will dominate the displacement becomes greater. Eventually, at a sufficiently high value of I_{sc} the most probable wavelength dominates the displacement and the displacement is said to be pseudostable [19, 26, 36]. If the displacement is pseudostable, the perturbation velocity of a finger is thrice that of the critical perturbation velocity associated with the actual injection rate [19]. That is, the velocity of the most probable finger is given by

$$\left(v^*_{wm}\right)_o = \frac{3\, v\, (M - 1 - N_g)}{2} \left(\frac{M^{2/3} - 1}{M^{2/3}} \right) \tag{94}$$

Consequently, the breakthrough recovery for a pseudostable displacement can be demonstrated to be

$$R_{bt} = \frac{1 - S_{wi} - S_{or}}{1 - S_{wi}} \left[\frac{Z_o}{L} + \frac{1 - Z_o/L}{1 + 3\, \frac{M - 1 - N_g}{2} \cdot \frac{M^{2/3} - 1}{M^{2/3}}} \right] \tag{95}$$

5. EXPERIMENTAL EQUIPMENT, PROCEDURE AND VARIABLES OF INTEREST

5.1 Description of the Experimental Apparatus

A schematic diagram of the equipment used in the experiments conducted to validate the stability theory is shown in Figure 1. The experimental set-up was similar to the one used in a previous study [27]. The circular coreholder, of an inner diameter of 6.31 cm and a total length of 100 cm, was made of aluminum. The two end-caps were designed in such a way as to achieve an even distribution of the injected liquid across the entire cross-section of the core. The end caps were filled with large glass beads which were held in place by a fritted glass plate made of fused glass beads. A Ruska Pump was used to obtain a constant injection rate of the desired magnitude over the range of 2.5 cc/hr to 1120 cc/hr. The pressure differentials across the length of the core were measured by a pressure transducer capable of sensing pressures up to 50 psig.

5.2 Experimental Procedure

The experimental procedure can be divided into three distinct parts: core-packing methodology, core property determination and displacement procedure. Each part of the procedure is described in detail in the following sections.

5.2.1 Packing Procedure

The coreholder, the physical dimensions of which are listed in Table 2, was packed by means of the wet-packing method which yields sandpacks of consistent properties [37, 38]. After measuring the bulk volume of the coreholder, it was wet-packed in the following manner. The coreholder was filled partially with distilled water, followed by dry 80 - 120 mesh, Ottawa silica sand of known quantity. Close packing of the sand grains was achieved by tamping the coreholder with a rubber hammer [32] for about an hour. After the vibration period, compressed dry air was

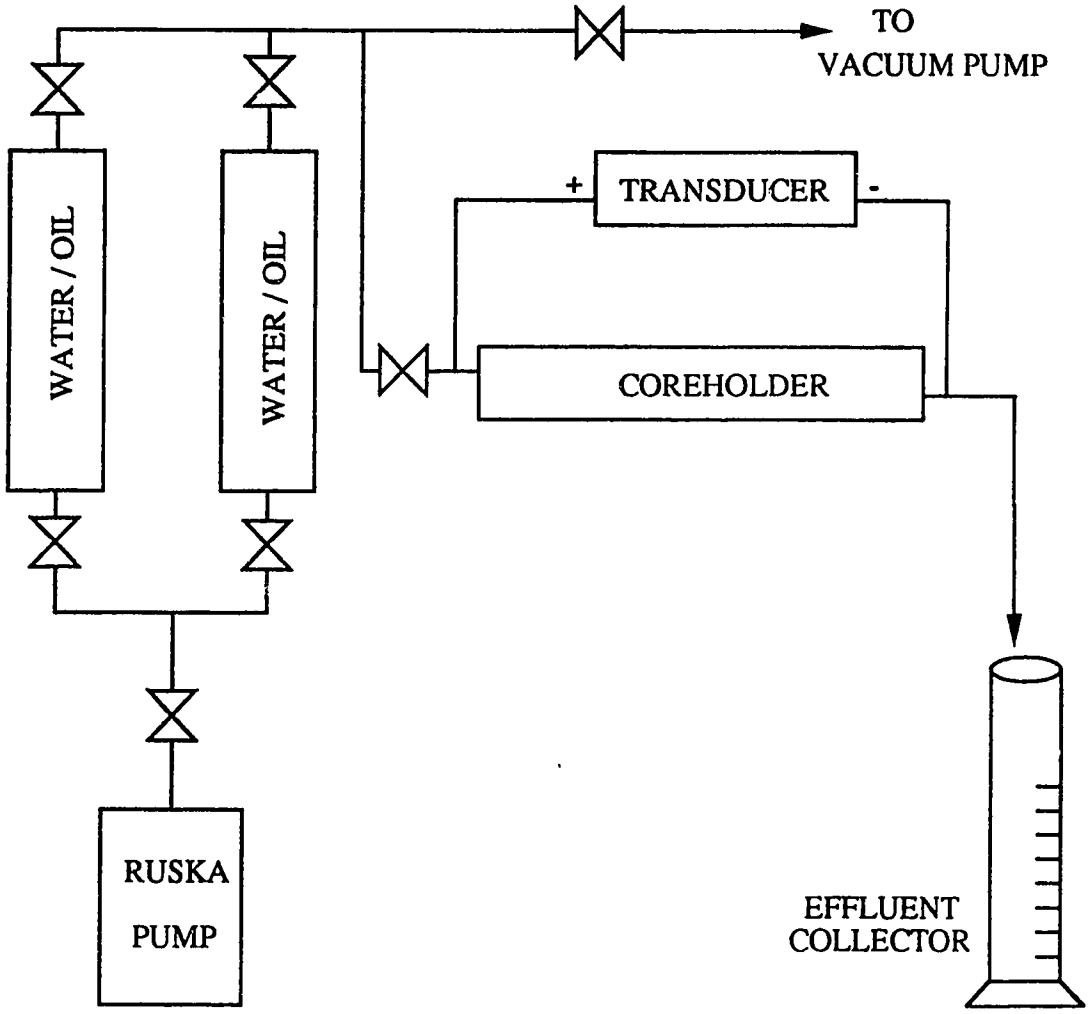

FIGURE1: SCHEMATIC OF DISPLACEMENT APPARATUS

passed through the coreholder for about 12 hours in order to remove most of the moisture in the core. The packed core was then attached to a vacuum pump and evacuated for 24 hours to ensure the complete removal of the packing water.

Table 2: Physical Dimensions of Coreholders

Bulk Vol. (cc)		Length Between Inlet and Outlet Pressure taps (cm)	Diameter (cm)
3100	100	99	6.30

5.2.2 Core Property Determination

In order to determine the core properties, the sandpack was placed in a vertical position and saturated with distilled water. The vertical position of the core was important for the simple reason that if any vapour did come off the water as it was introduced to the evacuated core, it would be easier to extract it from the system in that position. Also, no air would be trapped in the upper section of the core as could happen if the core was saturated in the horizontal position. The pore volume of the sandpack was then determined by a material balance calculation. Subsequently, the absolute permeability of the core was estimated using Darcy's law for several flow rates. The porosities and absolute permeabilities of the sandpacks are listed in Table 3.

Since the system used in this study was a water-wet one, the initial water saturation was then established by displacing the water with the oil of interest. After the injection of approximately three pore volumes of oil, it was observed that the mobile water inside the core was removed completely. The initial oil in place (IOIP) and the initial water saturation were then determined by a material balance calculation. Subsequently, the permeability to oil at initial water condition was calculated by measuring the pressure differential across the core and using Darcy's law.

5.2.3 Displacement Procedure

After the sandpack properties were estimated, the flood was commenced with the displacing fluid being either distilled water or distilled water doped with 0.1% sodium fluorescein. The latter was used as the displacing fluid in Runs 11 and 12 only. The displacement was stopped at water breakthrough in order to photograph the core cross-sections under ultra-violet light. The flood was conducted in the following manner. The inlet end of the horizontal coreholder was connected to the water bomb. A graduated cylinder was placed at the outlet to the collect the effluent. An appropriate injection rate was selected by choosing the correct gear ratio on the Ruska Pump. The

Table 3: Porosities and Absolute Permeabilities of Sandpacks

Runs	Porosity (fraction)	Absolute Permeability (d)
1	0.3548	13.27
2	0.3565	12.38
3	0.3550	13.20
4	0.3548	12.38
5	0.3613	12.59
6	0.3565	13.03
7	0.3419	12.18
8	0.3645	13.03
9	0.3548	13.27
10	0.3581	12.81
11	0.3581	12.59
12	0.3629	13.03
13	0.3548	12.92
14	0.3581	13.03
15	0.3613	13.03
16	0.3548	12.59
17	0.3516	12.81
18	0.3581	12.59
19	0.3565	13.03
20	0.3516	12.38
21	0.3548	13.03
22	0.3581	12.81
23	0.3565	13.27
25	0.3548	12.38

displacement, at this constant rate, was continued until the breakthrough of water, i.e., when the first drop of water reached the outlet end. Thus, the breakthrough recovery of oil could be calculated, as a fraction of the IOIP. The flood was continued until three to four pore volumes of water were injected, at which time, the incremental recovery of oil from the core was observed to be zero. From material balance calculations, the residual oil saturation within the core was determined. Finally, the permeability to water at residual oil saturation was calculated by measuring the pressure drop across the length of the core, and by using Darcy's law.

5.3 Photography of Core Cross-Sections

One of the objectives of this study was to attempt to determine, with a certain degree of certainty, where a finger was initiated. To this end, a technique, which has been used in previous studies [18, 32], was adopted whereby the core cross-sections, after water breakthrough, were photographed under ultraviolet lighting.

Runs 11 and 12 were terminated after water breakthrough and several sections of the core were retrieved from the coreholder and photographed under ultraviolet lighting using a yellow filter. In the resulting photographs, the bright white areas indicate the areas of the core cross-sections swept by the fluorescent displacing water, while the dark patches are the areas uncontacted by the water.

5.4 Variables of Interest

In order to determine the values of the instability number and the breakthrough recoveries for stable and pseudostable displacements, there were several fundamental variables which needed to be estimated or known. These variables could be classified as follows.

(1) Fundamental Material Property Variables

The fundamental material property variables were the following.

(i) μ_o, μ_w, the viscosities of oil and water, respectively, at room temperature;

(ii) A_c, the area under the capillary pressure versus saturation curve, which is a function of wettability, interfacial tension and pore-size distribution [22, 27]. The values of A_c for different fluid pairs were taken from Reference 27, as the porous medium and the fluids used in that study were the same as those in the present study.

(2) Fundamental Experimental Variables.

The fundamental experimental variables were the following.

(i) V_3, the bulk volume of the core which was measured directly;

(ii) L, the length of the core;

(iii) V_1, V_2, the input and output volumes of water, respectively, which were used to determine the pore volume (V_p) of the core;

(iv) V_4, the total volume of water produced from the core at the end of the oilflood which was used to calculate the initial water saturation (S_{wi});

(v) Q_o, ΔP_1, the flow rate of oil and the corresponding stabilized pressure drop, respectively, which were used to estimate the permeability of oil at initial water saturation (k_{oiw});

(vi) Q, the flow rate at which the displacement of oil by water was carried out;

(vii) R_t, the recovery of oil at water breakthrough;

(viii) Z_o, the distance from the inlet end of the core where fingering began;

(ix) V_5, the total volume of produced oil, measured at the end of the waterflood which was used to estimate the residual oil saturation (S_{or});

(x) Q_w, ΔP_2, the flow rate of water and the corresponding stabilized pressure drop, respectively, which were used to determine the permeability to water at residual oil saturation (k_{wor}).

Thus, a maximum of sixteen fundamental variables were required to be known or estimated, in order to calculate the values of the instability number (I_{sc}) and the breakthrough recovery (R_{bt}) for every experimental run.

6. EXPERIMENTAL RESULTS AND DISCUSSION

6.1 Introduction

The immiscible displacements carried out in this study were conducted in water-wet unconsolidated sandpacks. Two different fluid pairs having viscosity ratios of 29.60 and 61.28 were used in this study. The different properties of these fluids are listed in Table 4. The experiments were carried out over a wide range of displacement rates, from 5 cc/hr to 2800 cc/hr. The data from these experiments enabled the validation not only of the stability boundary, but also of the equations used to estimate the breakthrough recovery for stable and pseudostable displacements. Moreover, the equation used to estimate the pseudointerfacial tension has been validated experimentally.

The actual (calculated average) and predicted breakthrough recoveries for stable and pseudostable displacements for the two different viscosity ratios used in this study are reported in Table 5. The displaced fluid (oil) in one-half of the 24 experiments conducted in the present study was MCT-5, and in the remaining dozen was MCT-10. The end-point saturations and permeabilities for displacements with MCT-5 and MCT-10 are given in Tables 6 and 8, respectively, and the displacement data in Tables 7 and 9, respectively. The end-point permeabilities for Run 3 could not be calculated because of transducer malfunction. Runs 11 and 12 were stopped at water breakthrough in order to photograph the core cross-sections to estimate the distance from the inlet end of the core to where fingering was initiated. This distance (Z_o) was then used in Equations 92 and 95 to predict the stable and pseudostable breakthrough recoveries for the two different viscosity ratios studied. The breakthrough recovery as a fraction of the IOIP is plotted as a function of the instability number in Figure 2.

6.2 Results

Some of the important results observed from the experiments are described in detail in the following sections.

Table 4: Fluid Properties at 22°C

Fluid System	Density* (gm/cc)	Viscosity (cp)	Interfacial tension (dyne/cm)	Ac* (dyne/cm^2)
1. Distilled Water	0.9982	1.028	-	-
2. MCT-5	0.8123	30.43	33.2	16341
3. MCT-10	0.8576	63.00	34.3	13573

* from Reference 27

Table 5: Actual and Predicted Breakthrough Recoveries

Fluid System	Viscosity Ratio	Stable breakthrough recovery (% of IOIP)		Pseudostable breakthrough recovery (% of IOIP)	
		Predicted	Actual	Predicted	Actual
1. MCT-5 and Distilled Water	29.60	49.95	50.00	42.81	-
2. MCT-10 and Distilled Water	61.28	39.13	39.01	37.14	36.37

Table 6: End-Point Saturations and Permeabilities for MCT-5 Displacements

Runs	S_{wi} (% of pore volume)	k_{oiw} (d)	S_{or} (% of pore volume)	k_{wor} (d)
1	10.91	8.31	18.00	1.85
2	12.22	9.48	23.98	1.95
3	11.93	-	22.60	-
4	11.27	9.37	23.64	1.95
5	11.16	8.94	19.20	2.12
6	11.04	8.24	20.18	1.90
7	10.38	7.51	25.47	1.67
8	12.57	8.17	26.55	1.90
9	10.91	9.87	21.82	2.21
10	11.71	8.54	20.72	1.89
11	11.26	8.30	-	-
12	11.56	8.37	-	-

Table 7: Displacement Data for MCT-5 Displacements

Runs	Q (cc/hr)	IOIP (cc)	M	σ_e (dyne/cm)	I_{sc}	R_{bt} (% of IOIP)
	560	983	6.59	4122	97.13	43.88
2	50	970	6.09	3717	8.41	50.00
3	50	974	-	3798	-	49.90
4	50	976	6.16	3774	8.38	49.89
5	80	995	7.02	4111	12.95	50.25
6	100	983	6.83	4006	18.03	49.03
7	400	950	6.58	3584	88.25	45.05
8	200	988	6.88	3626	40.13	47.06
9	5	980	6.63	3900	0.772	49.80
10	10	980	6.55	3953	1.76	50.20
11	100	985	-	-	-	45.18
12	100	995	-	-	-	45.33

Table 8: End-point Saturations and Permeabilities for MCT-10 Displacements

Runs	S_{wi} (% of pore volume)	k_{oiw} (d)	S_{or} (% of pore volume)	k_{wor} (d)
13	11.09	10.34	24.55	4.28
14	10.90	10.23	24.95	4.13
15	12.50	10.14	23.93	4.17
16	11.09	10.12	25.45	4.18
17	11.00	10.20	26.51	4.19
18	12.80	10.30	23.42	4.24
19	11.04	10.14	25.16	4.15
20	11.00	10.31	24.95	4.25
21	10.91	10.16	24.91	4.15
22	11.08	10.13	24.50	4.18
23	11.76	10.23	23.98	4.17
24	11.91	10.22	24.09	4.42

Table 9: Displacement Data for MCT-10 Displacements

Runs	Q (cc/hr)	IOIP (cc)	M	σ_c (dyne/cm)	I_{sc}	R_{bt} (% of IOIP)
13	100	978	25.37	3100	37.75	38.24
14	560	989	24.74	3117	212.63	37.00
15	2400	980	25.20	3117	918.84	36.43
16	800	978	25.31	3056	312.97	36.50
17	1120	970	25.17	2982	445.55	36.29
18	2800	968	25.23	3100	1061.3	36.36
19	30	983	25.08	3087	11.60	38.96
20	40	970	25.26	3056	15.36	38.56
21	10	980	25.03	3091	3.85	39.08
22	1600	987	25.29	3131	610.47	36.47
23	2000	975	24.98	3109	761.15	36.31
24	5	969	26.50	3082	1.92	39.00

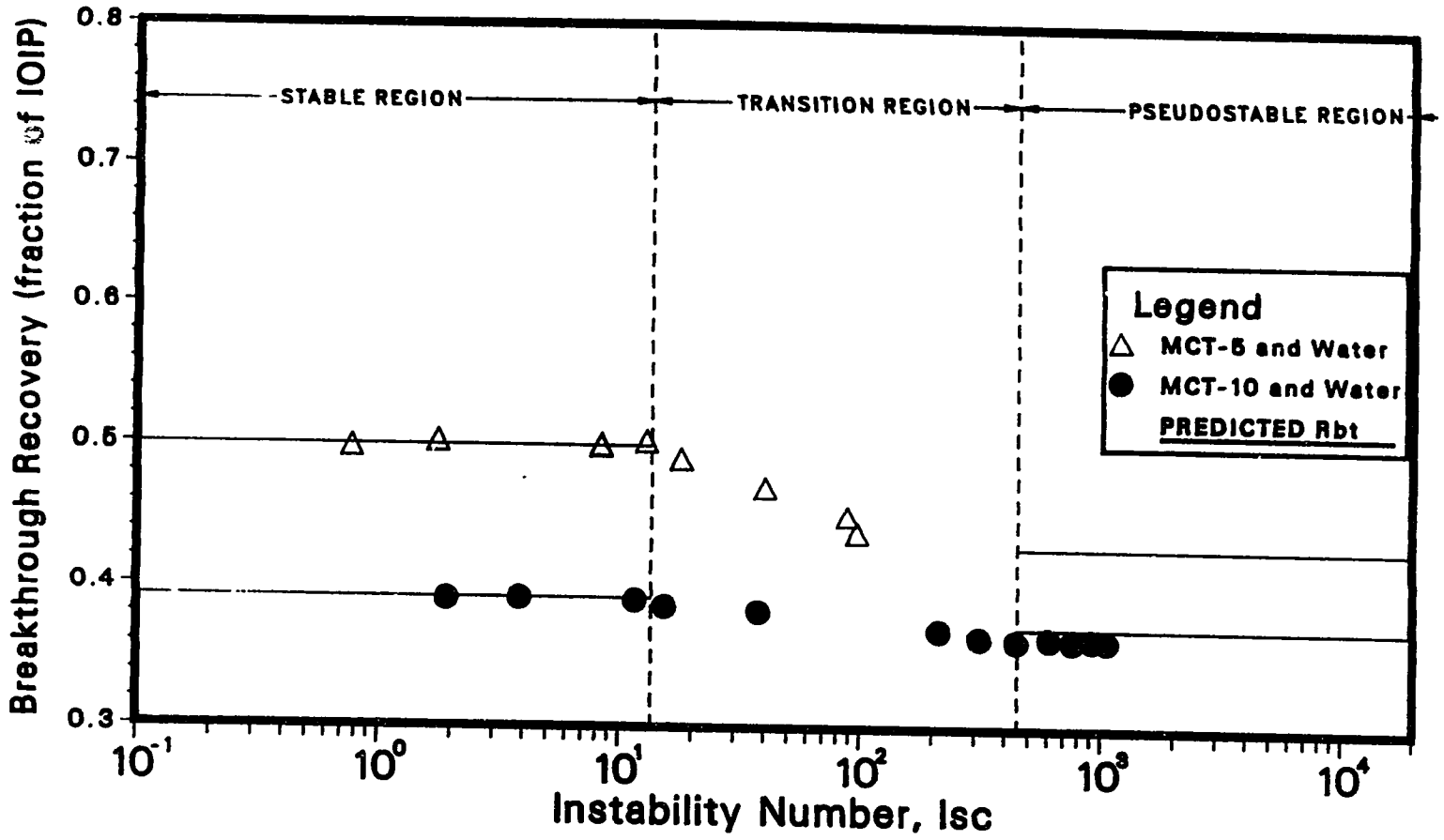

FIGURE 2: BREAKTHROUGH RECOVERY AS A FUNCTION OF INSTABILITY NUMBER

6.2.1 Displacement Records

The first twelve displacement runs in the present study were conducted with MCT-5 as the displaced fluid and the corresponding data are tabulated in Table 7. It can be observed from Table 7 that for Run 6, which was carried out at a displacement rate of 100 cc/hr, the instability number was 18.03, which was the I_{sc} value (in the unstable region) closest to the stability boundary. Hence, in order to identify the location, along the length of the core, where the fingering phenomenon was initiated, Run 11 was performed at the same displacement rate as Run 6. The core cross-sections were photographed after the displacement process was stopped at water breakthrough.

The photographs of the core cross-sections at water breakthrough, from the inlet end of the core to 50 cm along its length, are presented in Plate 1. It can be observed from Frames 1 to 6 that the displacement was uniform at all cross-setions. However, as can be seen from Frame 7, severe oil bypassing commenced at a distance of about 50 cm from the inlet end of the core. In order to confirm this finding, Run 12 was performed at a displacement rate of 100 cc/hr and the same procedure was followed as before. It can be seen from Plate 2 that the recognizable pattern of viscous fingering started to develop again at a distance of 50 cm from the core inlet.

6.2.2 Stability Boundary

As can be seen from Equation 84, the stability of an immiscible displacement depends upon the diameter of the coreholder, and upon the mobility ratio, displacement rate and pseudointerfacial tension of the fluids used in the displacement. It can be observed from Figure 2 that there is good agreement between the theoretically predicted value of the stability boundary and that determined experimentally for the two different viscosity ratios used in the present study. Figures 3 and 4 have been used to indicate the prediction of the onset of instability in cylindrical systems in the studies by Peters [32], Demetre [37], Wiborg [40] and Baird [41].

FRAME 1:

FRAME

FRAME 5: 4

M INLET END

INLET END

M INLET END

FRAME 1: IN

FRAME 3: 20 (

FRAME 5: 40

INLET END

INLET END

INLET END

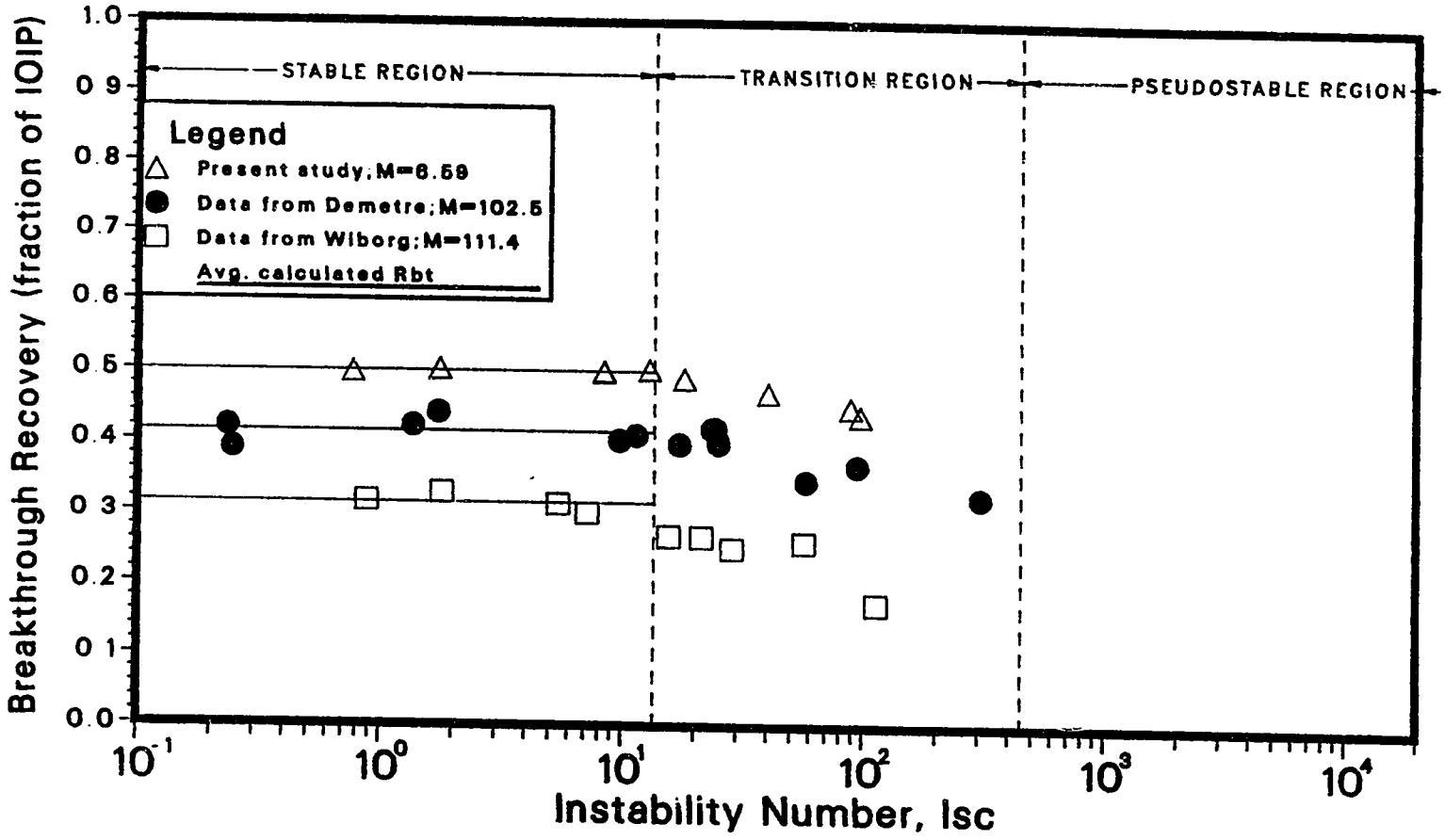

FIGURE 3: BREAKTHROUGH RECOVERY AS A FUNCTION OF INSTABILITY NUMBER; DATA FROM STUDIES BY DEMETRE & WIBORG

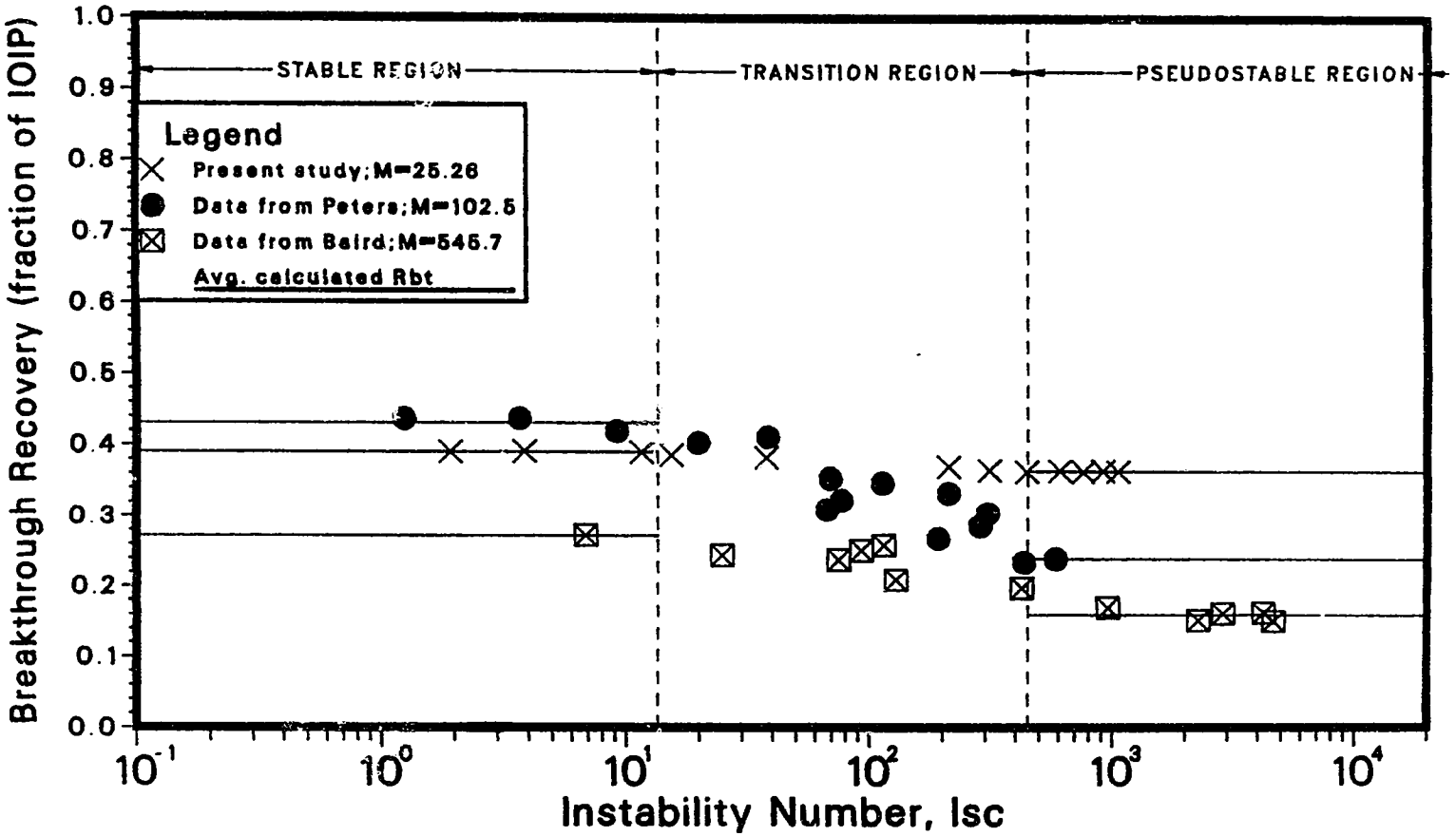

FIGURE 4: BREAKTHROUGH RECOVERY AS A FUNCTION OF INSTABILITY NUMBER; DATA FROM STUDIES BY PETERS AND BAIRD

The data from several runs in the above-mentioned studies, which are listed in Appendix B, were analyzed in order to calculate the instability number, I_{sc}, as given by Equation 84, for every run. In order to achieve this goal, the pseudointerfacial tension, σ_c, given by Equation 87, and, hence, the area under the capillary-pressure-versus-saturation curve, A_c, for the particular rock-fluid system of interest had to be known or determined. To solve this problem, it was necessary to assume that A_c could be considered to be a product of C and σ, where C was a factor depending on the nature of the porous medium and σ was the interfacial tension between the fluids. An average value of C was found to be 409 cm^{-1} from Reference 27 and it was assumed that this value could be used to obtain the approximate values of A_c for the different systems used by Peters [32], Demetre [37], Wiborg [40] and Baird [41], provided the values of σ were known. The values of I_{sc} from these four studies, thus calculated, were plotted in Figures 3 and 4 against the observed values of the breakthrough recovery as fractions of the IOIP.

6.2.3 Onset of the Pseudostable Region

For a particular rock-fluid system, when the displacement rate is large so that the magnitude of I_{sc} falls within the pseudostable region, then, as in the stable region, the recovery is independent of I_{sc} [27, 37, 38]. Demetre [37] has shown, using his data and also data from the study carried out by Peters [32], that the onset of the pseudostable behaviour occurs at a stability number of 900. Now, the instability number, developed in the present study and given by Equation 84, is proportional to the one derived by Peters and Flock [18]. The constant of proportionality, $C_c(M)$, is given by Equation 85. Thus, if $C_c(M)$ is taken into consideration when determining the onset of the pseudostable region, one would expect an instability number differing from that reported by Demetre [37] by the factor, $C_c(M)$. The reasons for this difference are two-fold. First, the present theory is based on the force potential approach; and, unlike

the velocity potential approach of Peters and Flock [18] or Demetre, this theory can account for the relative widths of the oil and water fingers as will be discussed in detail later in Section 6.3. Second, in the experiments conducted by Peters and Flock and Demetre, the displacements were terminated at water breakthrough and not at residual oil conditions. Moreover, in these studies, in the equation for the stability number, the permeability to water at residual oil saturation was approximated by the absolute permeability. These factors in combination might have been the major reason for the noise in the displacement data in these studies.

For M = 25.26, the value of $C_c(M)$ is 0.558; and hence, if this factor is taken into consideration, then the instability number at which the onset of the pseudostable region occurs becomes (900) · (0.558) = 500. This agrees fairly closely with the experimental observations which are plotted in Figure 2, from which it can be seen that the pseudostable region begins at an I_{sc} value of about 450. It is to be noted that an identical value of the instability number was found to coincide with the onset of pseudostable behaviour for rectangular systems [27].

6.2.4 Breakthrough Recovery

Knowing the perturbation velocity of a water finger, given by Equation 71, the equations for the breakthrough recovery of oil for stable (Equation 92) and pseudostable (Equation 95) displacements were derived. Equation 92 was derived with the assumption that the superficial velocity of the displacement was such that I_{sc} was only slightly greater than 13.56, and the only wavelength possible was that associated with the critical eigenvalue, γ_c [23]. Equation 95 was developed by assuming that the wavelength associated with the most probable eigenvalue, γ_m, was the one that was propagating through the system.

Using Equations 92 and 95, the breakthrough recoveries for stable and psueodstable displacements were calculated for the two different fluid pairs used in this

study. As can be seen from Table 5, it would appear that the predicted values for breakthrough recovery of a stable displacement are in good agreement with the average values determined experimentally for the two viscosity ratios of interest, with the maximal difference between the predicted and the actual values being about 2%. The variation in the observed breakthrough recovery for stable displacements (the range in the calculated values of stable R_{bt} being, on the average, about 0.6% of the mean calculated stable R_{bt}), as may be seen from Figure 2, may be attributed to two major reasons. First, the end-point mobility ratio varied from run to run because of variations in the end-point saturations. Second, the variability due to packing and the geological properties of the sand had an effect on the breakthrough recovery, as will be seen later in Section 7 of this report.

For the displacements with MCT-5, for which the average calculated mobility ratio was 6.59, it was not possible to conduct displacements at high values of the instability number, because of equipment limitations (very high flow rates and small pore volumes of the sandpack). However, because of the higher mobility ratio encountered (M = 25.26) during displacements with MCT-10, it was possible to go beyond the pseudostability boundary. The predicted breakthrough recovery for pseudostable displacements matched fairly closely with the average calculated breakthrough recovery for the MCT-10 displacements, with the difference being about 2% of the actual pseudostable R_{bt}.

6.3 Discussion

One of the significant achievements of the present study is the successful extension, to cylindrical porous media from rectangular systems, of the stability theory of Bentsen [19] to predict the onset of instability and the breakthrough recovery for stable and pseudostable displacements. According to the present theory, the instability

number, I_{sc}, and its critical value beyond which the displacement becomes unstable, for cylindrical systems, are given by Equation 84.

As can be seen from Figures 2, 3 and 4, the dimensionless group, I_{sc}, divides the displacement domain in a cylindrical core into a stable, an unstable and a pseudostable region. When I_{sc} is less than 13.56, the displacement is stable, whereas when it is greater than 13.56 and less than about 450, the displacement is unstable. Beyond the I_{sc} value of 450, the displacement is pseudostable.

In the defining equation for the instability number (Equation 84), the term $(M - 1 - N_g)$ arises because of the force balance carried out on the interface. In particular, the term $M - 1$ arises because of the contribution of the mobility contrast to the pressure difference across the interface, while the term N_g arises out of the density contrast across the interface. The term $C_c(M)$ appears in Equation 84 because of the fact that when the mobility of the displaced fluid is less than that of the displacing fluid, the width of a finger of the driving fluid is greater than that of the contiguous, oppositely directed finger of the driven fluid [19, 26]. This additional factor, $C_c(M)$, did not appear in the stability number proposed by Peters and Flock [18] because when the velocity potential approach is taken, one cannot determine how rock and fluid properties might affect the displacement process [19]. The correction factor in the instability number of rectangular systems has been shown to be given by Equation 86. Comparing Equations 85 and 86 it can be seen that the correction factor in the instability number depends upon the geometry of the coreholder.

Figure 5 shows the dependence of C_c (M) and C_r (M) on the mobility ratio, M. As can be seen from Figure 5, when M changes from 1 to ∞, C_c (M) varies gradually from 1 to 0.5 and C_r (M) from 1 to 4. Thus, there is a significant difference between these functions as far as their dependence on mobility ratio is concerned. Now, the instability number for cylindrical systems has been validated in the present study. Moreover, the instability number of rectangular systems has also been verified by

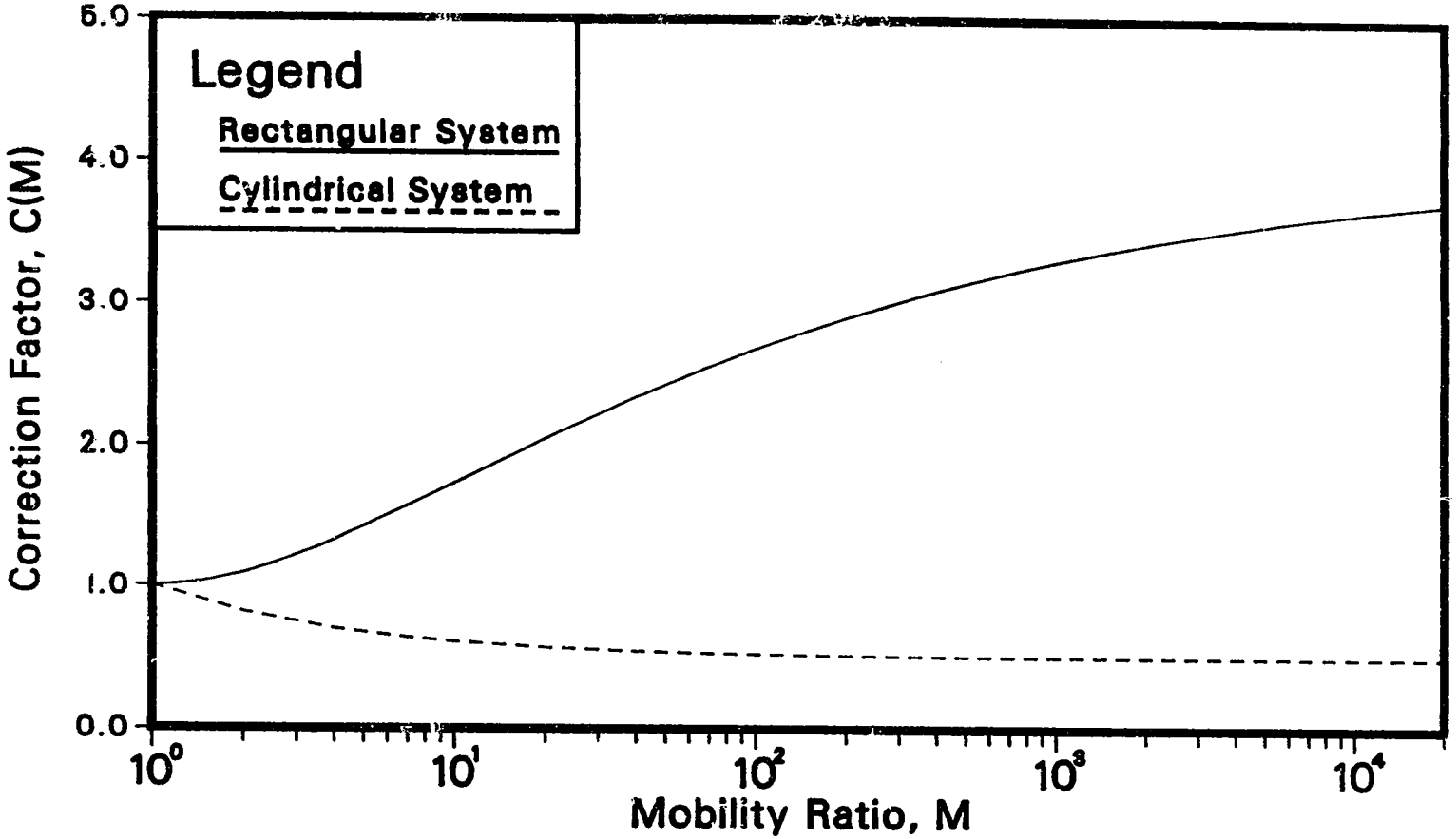

FIGURE 5: CORRECTION FACTOR AS A FUNCTION OF MOBILITY RATIO

means of experimental data [26]. Hence, it may be concluded that in spite of the correction factors differing markedly, the fact that the instability numbers for these two systems have been validated experimentally shows, at least indirectly, that the pseudointerfacial tension, σ_e, which has been used in the defining equations of both of these instability numbers, has been defined correctly.

The pseudointerfacial tension, given by Equation 87, was defined by assuming that the transition region (capillary fringe) separating the oil from the water could be replaced with a continuous, smooth pseudosurface to which the macroscopic radii of curvature could be extrapolated. Moreover, the pseudointerfacial tension was defined in terms of the area under the capillary pressure curve, A_c, which was supposed to have units of erg/cm^3. Even though this supposition is correct when considering units, from the physics viewpoint, A_c should have units of erg/cm^2/cm, where the unit of cm refers to the thickness of the capillary fringe surrounding the central core of the water finger [42]. It has been shown recently by Bentsen [42] that, by including the thickness of the capillary fringe and by using Gibbs' theory of surface tension, the pseudointerfacial tension may be defined by

$$\sigma_e = A_c \phi (1 - S_{wi} - S_{or}) w_s \tag{96}$$

where w_s refers to the average thickness of the capillary fringe. From a comparison of Equations 87 and 96, it may be observed that for these two equations to be equivalent, the thickness of the capillary fringe, w_s, should be equal to 1 cm.

As has been discussed in Sections 4.7 and 4.12, the stability boundary for an immiscible displacement process in cylindrical pores can be obtained by choosing m = 1 for the instability number, where m is the geometric mode number. This particular value of the mode number corresponds to the largest wavelength of the finger that can be accommodated by the porous medium. At higher values of the mode number, the

corresponding eigenvalues become larger, resulting in smaller values of the wavelength. The relationship between eigenvalue and wavelength of a water finger is given by

$$\lambda_w = \frac{2\pi}{\gamma_w} \tag{97}$$

Now, at different values of the mode number, the instability number will have different values. For example, for the values of m of 2, 3 and 4, the corresponding values of I_{sc} are 113.7, 291.5 and 548, respectively. This means that above the I_{sc} value of 113.7 the displacement will exhibit the second-mode configuration; that is, m = 2 gives the lower boundary of the second-mode, unstable displacement domain. It has been shown in Section 6.2.3 that the pseudostable region commenced at an I_{sc} value of about 450, and the closest integral value of m corresponding to this value of I_{sc} is 4.

Equation 80 enables the calculation of the time constant, n_w, for every eigenvalue, γ_w, for a particular value of superficial velocity, v. Although this relationship is continuous from the fluid mechanics point of view, in actual experiments only certain wavelengths, corresponding to the different values of the geometric mode number, are possible, owing to the finite size of the system. Figure 6 shows the time-constant-versus-wavelength plots for water and MCT-10 as the fluid pair (viscosity ratio of 61.28) for different values of the instability number. The number of points on each of these curves indicates the maximal mode number associated with that curve. For example, the curve corresponding to an instability number of 548 has four points and, hence, corresponds to m = 4. The point on the extreme left (on the curve) relates to the highest mode, which is the fourth mode for this particular curve. The point on the

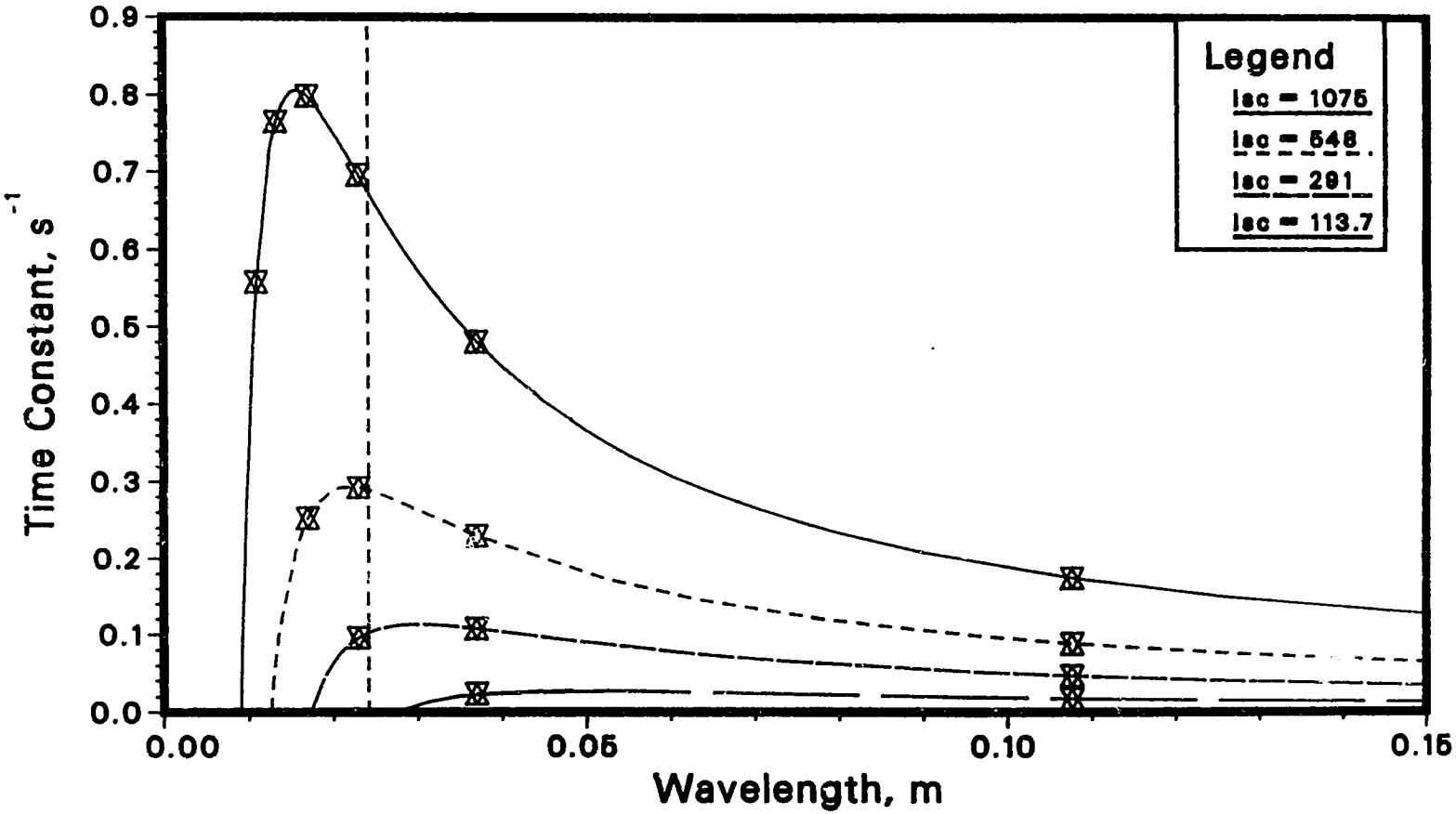

FIGURE 6: TIME CONSTANT AS A FUNCTION OF WAVELENGTH FOR THE FLUID PAIR OF WATER AND MCT-10

extreme right corresponds to the first mode, or the largest possible discrete value of the wavelength. For a particular value of the instability number, the most probable mode is the one, lying on the curve, having the maximal time constant.

From Figure 6 it can be observed that, for the curve corresponding to m = 4, the most probable mode is a smaller mode than the maximal mode for that curve. Thus, at an instability number of 548, the displacement should commence at the fourth mode, as at this mode there is enough energy to drive the perturbed interface at the corresponding wavelength [23]. However, later on, the displacement should shift to the third mode which has the greatest rate of surface creation among all the possible modes. At the third mode, three water fingers should propagate through the system, from a purely geometric point of view. In other words, for this particular fluid pair and porous media (diameter of 6.31 cm), three water fingers should be propagating through the system at the onset of the pseudostable behaviour. In a recent study conducted by Peters et al. [43], computer image processing techniques were used to count the population of water fingers per core cross-section at different degrees of instability. An empirical formula was developed in order to correlate the average number of fingers with the stability number. Using this formula, and by means of a relationship between I_{sc} and Peters' stability number, it was calculated that, at an I_{sc} of 450, the average number of fingers per core cross-section was about 2.3. Similarly, the average number of fingers amounts to 2.5 at an instability number of 548. This compares fairly well with the observation, made earlier in this paragraph, that three water fingers should be propagating through the system at the onset of the pseudostable behaviour. It should be noted, while making this comparison, that the relationship between time constant and wavelength of the fingers, and also the equations describing the fingers, are quite different for cylindrical systems, which have been used in this study, and rectangular systems, which were usedby Peters et al [43]. It may be argued that this difference in

the calculated values of the number of fingers may be due to the above-mentioned reasons.

From Figure 6 it can be seen that, with increasing instability number, the maximum of the plot of time constant versus wavelength gets sharper, and the probability that one particular mode dominates the displacement becomes greater. However, as has been observed experimentally in Reference 23, at high I_{sc} values the presence of microscopic heterogeneities in the porous medium may perturb and subsequently cause the mode configuration of the fingers to switch from a higher to a lower value. Now, the energy available in the system to drive the interface is constant for a constant displacement rate. When the fingers switch to a lower mode, some energy is released due to a reduction in the total surface area. This excess energy manifests itself by driving the resulting fingers at a higher rate [23].

Although in the present study no attempt was made to investigate the effect of variation of the core diameter on the stability problem, a few comments may be made on the effect of the core size on the plot of time constant versus wavelength. For different values of the core diameter, the superficial velocity, v, will have different values for the same volumetric flow rate, and hence the plot of time constant versus wavelength will be different and the values of the critical and most probable wavelengths will be different. Figure 7 is a plot of time constant versus wavelength, which has been obtained by using data from the study conducted by Demetre [37] who carried out experiments for cores having two different sizes. The smaller cores had an average diameter of 2.39 cm and the larger cores an average diameter of 4.851 cm. It can be seen from Figure 7 that, while the value of the time constant at any wavelength is greater for the smaller core, it is the third mode which is always closer to the peak of the curve than any other mode, irrespective of the size of the core.

It was observed in the study conducted by Demetre [37] that, for water-wet systems, the size of the core had no influence on the value of the stability number

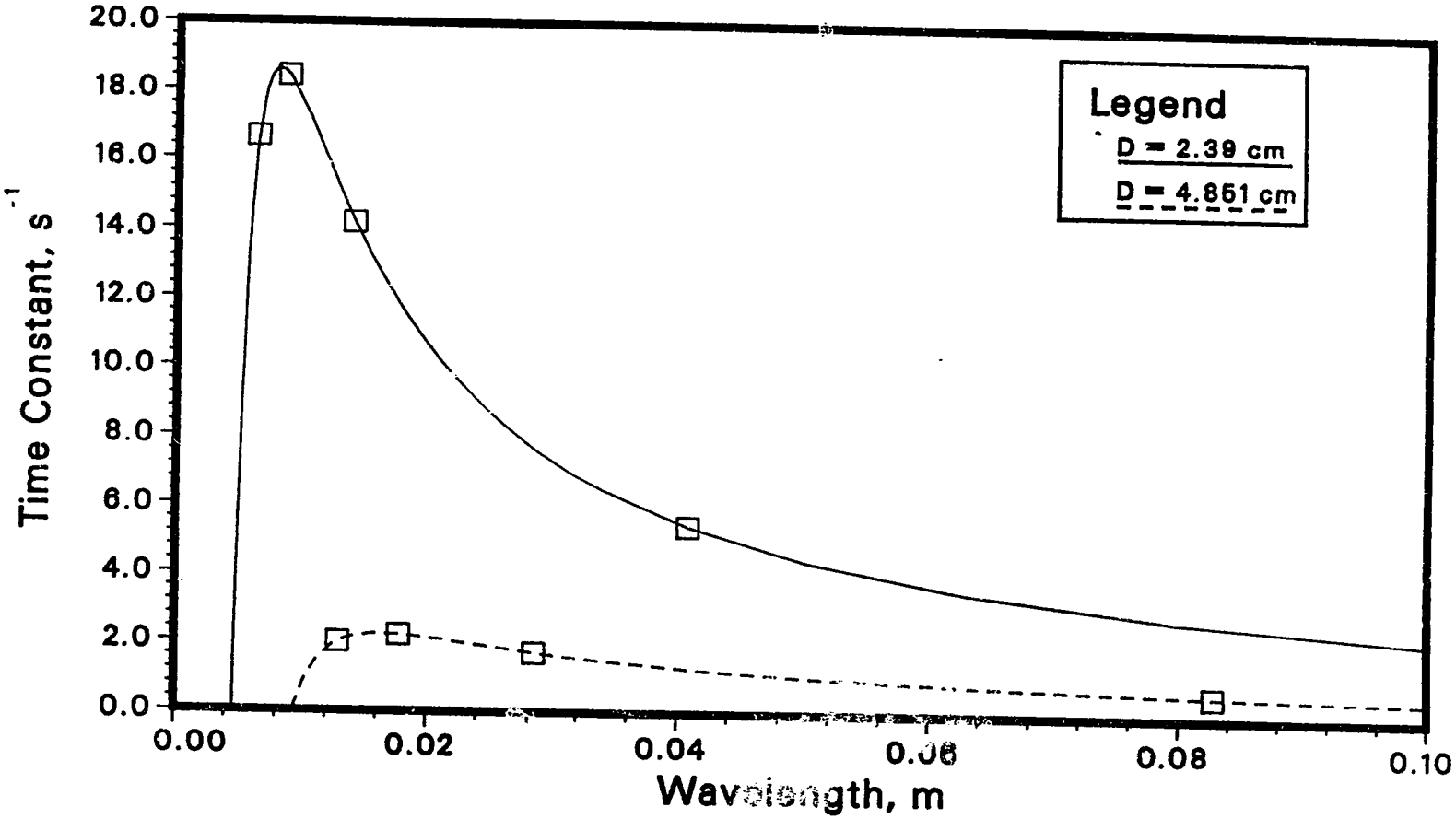

FIGURE 7: TIME CONSTANT AS A FUNCTION OF WAVELENGTH FOR TWO DIFFERENT CORE SIZES; Isc=548, M=102.5; DATA FROM DEMETRE

coinciding with the onset of the pseudostable region. However, as can be seen from Figure 7, for the two different diameters, the values of the time constant and wavelength are different at the peaks of the respective curves. This suggests that the onset of the pseudostable region is not brought about by the most probable wavelength but rather by the size of the propagating fingers. Now, the peak of the time-constant-versus-wavelength plot for the critical value of I_{sc} (i.e. $I_{sc} = 450$) may be shown to occur at a wavelength of about 0.0242 m for the particular system under consideration. As may be observed from Figure 6, for any I_{sc} value greater than the critical value of I_{sc}, the peak of the time-constant-versus-wavelength plot corresponds to a wavelength smaller than that corresponding to the peak of the curve for $I_{sc} = 450$. Hence, in order to explain the pseudostable behaviour of the displacement process, it may be argued that for I_{sc} values below the critical value, mode switching may take place from the highest to the lowest modes for any given unstable displacement. However, for I_{sc} values greater than 450, mode switching may take place only from the largest to the most probable modes and no further switches are possible. For example, for the uppermost curve in Figure 6, the most probable mode number is 4 and the maximal mode number is 6; hence, during the displacement process only two mode switches may take place.

Now, from a purely geometric point of view, the diameters of the dominant fingers propagating through the system can be calculated for different values of the maximal mode number, assuming that the cross-sectional shape of the fingers is circular. For example, for a maximal mode number of 2, the diameter of the fully developed finger, assuming it is circular, may be shown to be 2.27 cm for the particular core size used in the present study. It has been observed in this study that at the onset of the pseudostable region, which coincides with an I_{sc} value of 450, the dominant mode number of the displacement process is 3. The diameter of the dominant finger associated with the third mode is calculated to be about 1.42 cm. However, at this

point, it should be noted that in a real porous medium, because of local heterogeneities, local variations in σ_e, etc., the actual finger shape and size may be somewhat different from that considered in the present study. In the study conducted recently by Peters et al. [43], an empirical formula was developed to correlate the average cross-sectional area of viscous fingers with the stability number. Using this formula, for an instability number of 450, the average area of cross-section of a finger is calculated to be 4.96 cm^2, from which, assuming the finger has a circular shape, its diameter comes out to be about 2.51 cm.

This differs quite widely from the value of the finger diameter calculated before. The difference between these two values may, as mentioned earlier, be attributed to the differences in finger behaviour in rectangular and cylindrical systems.

7. SENSITIVITY ANALYSIS

7.1 Introduction

The instability number, I_{sc}, which is used to determine whether a given immiscible displacement of oil by water is stable or unstable, may be calculated by using Equation 84. The breakthrough recovery, R_{bt}, for any such stable or pseudostable displacement may be predicted by means of Equation 92 or 95, respectively. In ascertaining the magnitude of I_{sc} and R_{bt}, it is necessary to determine experimentally the value of each of their component variables. Moreover, each measurement of these variables involves experimental error, and each of these measurements contributes to the overall errors in the calculated values of I_{sc} and R_{bt}. In the present study, the estimated value of each of the component variables, together with its estimated standard error (which will be called standard deviation in this study), have been used to perform an error (sensitivity) analysis, both analytically and numerically, on the calculation of I_{sc}. In addition, the relative contribution of each of the different components to the total bias and variance has been estimated. A similar analysis has been performed numerically on the calculation of R_{bt}.

However, it is to be noted that the above analysis is valid only for a single determination of I_{sc} or R_{bt} and, hence, the errors involved are with respect to a single, non-reproducible experiment with a given sample of sandpack. The total variance with respect to general experimental determination of I_{sc} (and R_{bt}) must include, in addition, the variability attributable to the material properties of the sandpack sample and the packing procedure. Consequently, an attempt has also been made in this study to estimate the contributions of both the variability due to the packing procedure and the geological characteristics of the sand to the total experimental variability. In order to achieve this goal, data from two replicate runs (Runs 2 and 4) have been used.

7.2 Mathematical Model

The basic problem is as follows. Given $y = f(X_1, X_2, X_3, ..., X_n)$, where f is any single-valued function of n variables, then the individual mean value may be estimated using

$$\overline{X}_i = \frac{\sum X_i}{N} \tag{98}$$

where N is the number of observed values of variable X_i. Let $E(X_i)$ be the expected value of i^{th} component variable (i = 1, 2, ..., n) and E(y) be the expected value of y. The expected value of any continuous function g(X) is defined as [44]

$$E[g(X)] = \int_{-\infty}^{+\infty} g(x)\, f_X(x)\, dX \tag{99}$$

where

$$F_X(x) = P(X \leq x), \quad -\infty < X < \infty \tag{100}$$

and

$$f_X(x) = \frac{d\, F_X(x)}{dX} \tag{101}$$

Here, X is a random variable, x is a particular value in the set of all possible values of X, $P(X \leq x)$ is the probability that X will take on a value less than or equal to the

particular value x and $f_X(x)$ is the probability density function of the continuous variate X.

Now, considering two different input variables X_i and X_j, the estimator of the second moment of the variables may be defined by [45]

$$S_{ij} = E[X_i \cdot X_j] - E[X_i] \cdot E[X_j] \tag{102}$$

where

$$E[X_i \cdot X_j] = \int_{-\infty}^{+\infty} \int_{-\infty}^{+\infty} x_i x_j f_{X_i,X_j}(x_i, x_j)\, dx_i\, dx_j \tag{103}$$

If X_i and X_j are statistically independent, one can write Equation (103) as

$$E[X_i \cdot X_j] = \int_{-\infty}^{+\infty} x_i f_{X_i}(x_i)\, dx_i \cdot \int_{-\infty}^{+\infty} x_j f_{X_j}(x_j)\, dx_j = E[X_i] \cdot E[X_j] \tag{104}$$

By introducing Equation 104 into Equation 102, it follows that $S_{ij} = 0$. In other words, when $S_{ij} = 0$ for $i \neq j$, the variables are statistically independent. When $i = j$, S_{ij} is written as S_i^2, where S_i^2 is an estimator of the variance of the i^{th} variable. Similarly, $S_{X_i}^2$ is an estimator of the variance of X_i.

Now, considering the equation $y = f(X_1, X_2, X_3, ..., X_n)$, it is assumed that the component variables are uncorrelated. Then, expanding $f(X_1, X_2, X_3, ..., X_n)$ in a multivariable Taylor Series up to second order (leaving out the 3rd and higher order terms) about $[\overline{X}_1, \overline{X}_2 ..., \overline{X}_n]$, one gets, after simplifying [46],

$$E[y] \cong f(\overline{X}_1, \overline{X}_2, \ldots, \overline{X}_n) + \frac{1}{2}\sum_{i=1}^{n}\left(\frac{\partial^2 f}{\partial X_i^2}\right)_{\overline{X}_i} S_{X_i}^2 \qquad (105)$$

and

$$VAR(y) \cong \sum_{i=1}^{n}\left(\frac{\partial f}{\partial X_i}\right)_{\overline{X}_i}^2 S_{X_i}^2 \qquad (106)$$

where VAR(y) is the variance of y and the subscript $\overline{X}_i$ means that the terms are evaluated at the average values of the component variables. The second term in the right-hand side of Equation 105 will be called the bias in the estimation of y.

Equations 105 and 106 apply to any function. The only restriction is that all the measured quantities indicated by X's are statistically independent. The equation for VAR(y) (or S_y^2) provides a method for estimating the total variance of a function and, hence (assuming that one can measure precision in terms of second central moments), the total precision of the calculated result. It is also a method for determining which component of the function makes the largest contribution to the variance of the total, and therefore points the way both to where the maximal improvement can be effected and where it is fruitless to attempt an improvement in the precision.

The application of the propagation of variance formula involving the derivatives is illustrated by means of the following example. The porosity of a core is defined as $\phi = \frac{V_p}{V_b}$, where V_p is the pore volume and V_b is the bulk volume of the core. Then, in order to make an analytical evaluation of the variance of ϕ, the values of the squares of the partial derivatives of ϕ with respect to its two component variables need to be determined. The partial derivative of ϕ with respect to V_p at the mean values of the variables is given by

$$\frac{\partial \phi}{\partial V_p} = \frac{1}{\overline{V}_b} = \frac{\overline{\phi}}{\overline{V}_p} \tag{107}$$

so that

$$\left(\frac{\partial \phi}{\partial V_p}\right)^2 S^2_{V_p} = \frac{\overline{\phi}^2}{\overline{V}^2_p} S^2_{V_p} \tag{108}$$

Similarly, the square of the partial derivative of ϕ with respect to V_b at the mean values of the variables is

$$\left(\frac{\partial \phi}{\partial V_b}\right)^2 S^2_{V_b} = \frac{\overline{\phi}^2}{\overline{V}^2_b} S^2_{V_b} \tag{109}$$

Introducing Equations 108 and 109 into Equation 106, one obtains

$$S^2_\phi = \text{VAR}(\phi) = \overline{\phi}^2 \left(\frac{S^2_{V_p}}{\overline{V}^2_p} + \frac{S^2_{V_b}}{\overline{V}^2_b}\right). \tag{110}$$

The values of $\frac{S^2_{V_p}}{\overline{V}^2_p}$ and $\frac{S^2_{V_b}}{\overline{V}^2_b}$ indicate the relative contributions of the variables V_p and V_b, respectively, to the variance of the porosity, ϕ. The square root of the total variance gives the standard deviation in ϕ, S_ϕ. If one assumes that the probability distribution of ϕ is normal, then $\overline{\phi} \pm 1.96\, S_\phi$ gives the interval over which 95% of the experimental determinations of ϕ may be expected to occur [47]. Conversely, if one has determined a number of ϕ values whose range spans the above limit, then one may say that these values are not significantly different at the 5% level.

7.3 Formulas Used to Calculate I_{sc} and R_{bt}

As mentioned earlier in Section 5, there are a maximum of 16 fundamental variables which need to be measured or estimated, in order to calculate the values of the instability number and the breakthrough recovery. These variables have been defined already in Section 5. The formulas that are used to calculate the different parameters of interest, and finally the values if I_{sc} and R_{bt}, are as follows.

The porosity of a sandpack is defined as

$$\phi = \frac{V_1 - V_2}{V_3} \tag{111}$$

where V_1, V_2 and V_3 are the input and output volumes of water and the bulk volume of the core, respectively. The initial water saturation is calculated as

$$S_{wi} = \frac{\text{initial water volume}}{\text{pore volume}} = \frac{V_1 - V_2 - V_4}{V_1 - V_2} \tag{112}$$

where V_4 is the total volume of the mobile water in the core. The permeability to oil at initial water saturation is calculated as

$$k_{oiw} = \frac{Q_o \mu_o L^2}{V_3 \Delta P_1} \tag{113}$$

where Q_o and ΔP_1 are the flow rate of oil and the corresponding stabilized pressure drop measured across the length L of the core, respectively. The parameter μ_o is the oil viscosity. The residual oil saturation is estimated using

$$S_{or} = \frac{\text{residual oil volume}}{\text{pore volume}} = \frac{V_4 - V_5}{V_1 - V_2} \tag{114}$$

where V_5 is the volume of the mobile oil in the core. The permeability to water at residual oil saturation is given by

$$k_{wor} = \frac{Q_w \mu_w L^2}{V_3 \Delta P_2} \tag{115}$$

where Q_w and ΔP_2 are the flow rate of water and the corresponding stabilized pressure drop across the length of the core. The parameter μ_w is the viscosity of water. Using Equations 113 and 115, the mobility ratio of the displacement of oil by water may be defined as

$$M = \frac{k_{wor}\,\mu_o}{k_{oiw}\,\mu_w} = \frac{Q_w\ \Delta P_1}{Q_o\,\Delta P_2} \tag{116}$$

The pseudointerfacial tension may be defined, by introducing Equations 111, 112 and 114 into Equation 87, as

$$\sigma_e = \frac{A_c \cdot V_5}{V_3} \tag{117}$$

Now, the instability number for cylindrical systems is defined by Equation 84. Introducing Equations 115, 116 and 117 into Equation 84, the instability number may be expressed in terms of the fundamental variables as

$$I_{sc} = 87786.946\ \frac{\mu_w Q}{\left(\frac{Q_w \mu_w L^2}{V_3 \Delta P_2}\right)\left(\frac{A_c V_5}{V_3}\right)} \cdot \left(\frac{Q_w \Delta P_1}{Q_o \Delta P_2} - 1\right) \cdot \left[\frac{\left(\frac{Q_w \Delta P_1}{Q_o \Delta P_2}\right)^{2/3} + 1}{2 \cdot \left(\frac{Q_w \Delta P_1}{Q_o \Delta P_2}\right)^{2/3}}\right] \tag{118}$$

where μ_w is measured in cp, the flow rates, Q, Q_o and Q_w, are measured in cc/hr, the

pressure drops, ΔP_1 and ΔP_2, are measured in psi, the volumes, V_3 and V_5, are measured in cc and the area under the capillary pressure curve, A_c, is measured in dyne/cm^2. For stable displacements, the breakthrough recovery, expressed as a fraction of the IOIP, has been defined by Equation 92. Introducing Equations 112, 114 and 116 into Equation 92, one obtains, for the breakthrough recovery for stable displacements,

$$R_{bt} = \frac{V_5}{V_4}\left[\frac{Z_o}{L} + \frac{1-\frac{Z_o}{L}}{1+\frac{\left(\frac{Q_w\,\Delta P_1}{Q_o\,\Delta P_2}-1\right)}{2}\cdot\frac{\left\{\left(\frac{Q_w\,\Delta P_1}{Q_o\,\Delta P_2}\right)^{2/3}-1\right\}}{\left(\frac{Q_w\,\Delta P_1}{Q_o\,\Delta P_2}\right)^{2/3}}}\right] \qquad (119)$$

where all the variables are expressed in consistent units. It is to be noted that in both Equations 118 and 119, the gravity number, N_g, is considered to be equal to zero because of the fact that the system under consideration is horizontal.

7.4 Standard Deviations of the Component Variables

In order to evaluate analytically the standard deviation of I_{sc}, one has to determine the values of the partial derivatives of I_{sc} with respect to the component variables at the average values of these variables. Also, based on experimental observations, the mean values and the standard deviations of the component variables need to be estimated. These standard deviations, which actually are the standard errors of estimation of the relevant variables, have been estimated only on the basis of experience gained from Run 1. Hence, assuming each of these variables to be normally distributed, any particular value of such a variable has a 68% chance of lying within the range of plus- or minus-one standard deviation of the mean value of the variable.

From Equation 118 it can be seen that a maximum of ten fundamental variables need to be known in order to calculate I_{sc}. The average values (which, in fact, are the estimated values, based on data obtained from Run 1) of these variables and their standard deviations are listed in Table 10. As can be seen from Table 10, the error in measuring the viscosity of water is considered to be about 0.5%, because the room temperature (at which the viscosity of water was determined) was observed to remain nearly constant throughout the course of the experiment. Hence, there could not have been any significant variation in the value of μ_w. Similarly, because of the fact that the bulk volume of the coreholder was estimated directly by noting the volume of water required to fill up the empty coreholder completely, the measurement error is considered to be as low as 10 cc for a bulk volume of 3100 cc. The pressure differentials were measured using transducers, and the error of 0.01 psi was the maximum attained, once the pressures stabilized. The flow rates are considered to have errors of 0.05 cc/hr each, as the flow rates were governed by the gear-settings in the Ruska pump which yielded flow rates very close to the specified values.

7.5 Analytical Evaluation of the Standard Deviation of I_{sc}

The variance of I_{sc} can be calculated by considering all the component variables of I_{sc} given in Equation 118, and by using Equation 106. The mean values and the standard deviations of the component variables of I_{sc} are listed in Table 10. Noting, from Table 10, that $Q_w = Q_o = Q$, Equation 118 may be simplified to

$$I_{sc} = 87786.946 \frac{V_3^2}{A_c V_5 L^2} \frac{\left(\Delta P_1^{5/3} + \Delta P_1 \Delta P_2^{2/3} - \Delta P_1^{2/3} \Delta P_2 - \Delta P_2^{5/3}\right)}{2\,\Delta P_1^{2/3}} \qquad (120)$$

The partial derivatives of I_{sc} with respect to the component variables may be determined as follows. The first-order partial derivative of I_{sc} with respect of V_3 is

Table 10: Average Values and Standard Deviations of Variables Used to Calculate I_{sc}; Data from Run 1

Variables	Units	Estimated Values	Estimated Standard Deviations
μ_w	cp	1.028	0.005
Q	cc/hr	560.00	0.05
Q_w	cc/hr	560.00	0.05
ΔP_1	psi	26.47	0.01
Q_0	cc/hr	560.00	0.05
ΔP_2	psi	4.02	0.01
L	cm	99.0	0.10
V_3	cc	3100	10.00
A_c	dyne/cm^2	16341	10.00
V_5	cc	782	5

$$\frac{\partial I_{sc}}{\partial V_3} = 2 V_3 \frac{I_{sc}}{V_3^2} = \frac{2 I_{sc}}{V_3} \tag{121}$$

The first-order partial derivative of I_{sc} with respect to the area under the capillary pressure curve is given by

$$\frac{\partial I_{sc}}{\partial A_c} = - \frac{I_{sc}}{A_c} \tag{122}$$

The first-order partial derivative of I_{sc} with respect to V_5 may be shown to be

$$\frac{\partial I_{sc}}{\partial V_5} = - \frac{I_{sc}}{V_5} \tag{123}$$

The partial derivative of I_{sc} with respect to length is given by

$$\frac{\partial I_{sc}}{\partial L} = - \frac{2 I_{sc}}{L} \tag{124}$$

Finally, the partial derivatives of I_{sc} with respect of ΔP_1 and ΔP_2 may be demonstrated to be

$$\frac{\partial I_{sc}}{\partial (\Delta P_1)} = I_{sc} \frac{\Delta P_1^{4/3} + \frac{1}{3} \Delta P_1^{2/3} \Delta P_2^{2/3} + \frac{2}{3} \Delta P_1^{-1/3} \Delta P_2^{5/3}}{\Delta P_1^{5/3} \left(\Delta P_1^{5/3} + \Delta P_1 \Delta P_2^{2/3} - \Delta P_1^{2/3} \Delta P_2 - \Delta P_2^{5/3} \right)} \tag{125}$$

and

$$\frac{\partial I_{sc}}{\partial (\Delta P_2)} = I_{sc} \frac{\frac{2}{3}\Delta P_1 \Delta P_2^{-1/\beta} - \Delta P_1^{2/\beta} - \frac{5}{3}\Delta P_2^{2/\beta}}{\Delta P_1^{5/\beta} + \Delta P_1 \Delta P_2^{2/\beta} - \Delta P_1^{2/\beta}\Delta P_2 - \Delta P_2^{5/\beta}} \tag{126}$$

respectively. Using Equations 106 and 118, one obtains, for the standard deviation of I_{sc},

$$S_{I_{sc}} = \sqrt{VAR(I_{sc})} = \sqrt{a^2 S_{V_3}^2 + b^2 S_{A_c}^2 + c^2 S_{V_5}^2 + d^2 S_L^2 + e^2 S_{\Delta P_1}^2 + f^2 S_{\Delta P_2}^2} \tag{127}$$

where the values of a, b, c, d, e and f are given by Equations 121, 122, 123, 124, 125 and 126, respectively. Using Equation 120 and the mean values of the component variables, the mean value of I_{sc} may be obtained as

$$\overline{I}_{sc} = 97.13 \tag{128}$$

Introducing Equation 121 into 126 and the mean value of I_{sc} from Equation 128 into Equation 127, and using the mean values and the standard deviations of the component variables from Table 10, one obtains

$$S_{I_{sc}} = 0.9066 \tag{129}$$

It can be seen that the computation of the standard deviation of I_{sc}, and the calculation of the relative contributions of all the fundamental component variables to the variance in I_{sc}, involve a lot of time and effort, when done analytically. Similar computations for the bias of I_{sc} will require much more time and effort, if performed analytically, because of the need to determine second-order partial derivatives. These calculations may be done numerically, thus reducing the computational work by a

substantial amount. Also, after every cycle, the analysis can be redone as many times as desired with modified values of the arguments.

7.6 Numerical Evaluation of the Partial Derivatives

In the numerical method, the first- and second-order partial derivatives of I_{sc} and R_{bt} with respect to the different component variables are evaluated numerically. The method that has been used in the present study is as follows. If $S_{X_i} = 0$, then the bias and variance in the variable X_i are zero. Otherwise, five-point central differences are used to determine the first-order partial derivative at $\bar{X}_i$[48]. The points are spaced ($0.01\ S_{X_i}$) apart and are located centrally about $\bar{X}_i$. These five points are used to estimate the first-order partial derivatives to the left and to the right of $\bar{X}_i$. If the product of these left and right first-order derivatives is negative or zero, then the second-order partial derivative of the function at $\bar{X}_i$ is set to zero. Otherwise, the second-order partial derivative is calculated from the five points [48]. The bias and variance calculations are made using a Taylor series expansion of the function about its mean value, truncating all third- and higher-order terms. In order to perform a numerical evaluation of the partial derivatives of a function $f(X_1, X_2, ..., X_n)$ with respect to a variable X_i at any point $\bar{X}_i$, the following formulas are used. Let

$$h = 0.01\ S_{X_i} \tag{130}$$

Then the variance of the function may be calculated as

$$VAR = \sum_{i=1}^{n} \left\{ \frac{(f_{m_2} - f_{p_2}) + 8\,(f_{p_1} - f_{m_1})}{12\,h}\ S_{x_i} \right\}^2 \tag{131}$$

where f_{m_1}, f_{m_2}, f_{p_1} and f_{p_2} refer to the values of the function at ($\bar{X}_i - h$), ($\bar{X}_i - 2h$), ($\bar{X}_i + h$) and ($\bar{X}_i + 2h$), respectively. Again, let

$$d_{1l} = -3 f_{m_2} - 10 f_{m_1} + 18f - 6 f_{p_1} + f_{p_2} \tag{132}$$

where f is the value of the function at $\bar{X}_i$. Also, let

$$d_{1r} = -f_{m_2} + 6 f_{m_1} - 18 f + 10 f_{p_1} + 3 f_{p_2} \tag{133}$$

Here, d_{1l} and d_{1r} are the values of the partial derivatives of the function with respect to X_i to the left and to the right of $\bar{X}_i$, respectively. If $d_{1l} \cdot d_{1r} \leq 0$, then the second-order partial derivative of the function at the point of interest is set to zero. Otherwise, the second-order partial derivative is calculated as

$$d_2 = \frac{-(f_{m_2} - f_{p_2}) + 16 (f_{m_1} - f_{p_1}) - 30 f}{12 h^2} \tag{134}$$

Then, the bias in the function may be estimated using

$$\text{BIAS} = \sum_{i=1}^{n} \frac{d_2}{2} \cdot S_{\bar{x}_i}^2 \tag{135}$$

7.7 Description of the Program

The program, given in Appendix C, uses the method described in Section 7.6 for numerical calculation of the partial derivatives. Input of the number of function arguments, the names and units of these arguments, the name and unit of the function

result, and the statement of the function yields the function result together with its unit. Double-precision values of the arguments and their estimated standard deviations are then supplied, in list-directed mode, and the variance- and bias-component analysis table is produced by the program. The program is written in such a way that it recycles for possible argument modification. Modifications of the values of the arguments and their estimated standard deviations enable the user to repeat the analysis. For any particular estimate of a parameter and its standard deviations, the program allows the user to simulate the arguments as normal (Gaussian) or lognormal variates.

The main program is called "MAIN". The subprograms are called "REC", "DRAND", "RNORM", "RLOGN", "MNVRCP" and "FSORTI". "REC" is the only user-written routine here, and it returns a double-precision result from the values of the component variables. It is assumed that the function is defined throughout the practical simulation range of $X_i \pm 4S_{X_i}$ (i = 1, n), and is smooth enough that numerical differentiation at a spacing of (0.01 S_{X_i}) is valid. Subroutine "MNVRCP" accepts the arguments, the standard deviations of the variables and the function of interest, and performs numerical differentiation. Finally, the absolute bias and variance are calculated from a Taylor expansion of the function of interest (up to the second-order terms only) at the expected values of the variables. Function "DRAND" is a multiplicative, congruential generator of single-precision, uniformly distributed pseudo-random numbers. Function "RNORM" returns a double-precision, normal deviate of the mean and the standard deviation, whereas function "RLOGN" returns a double-precision, lognormal deviate of the mean and the standard deviation of the function. Subroutine "FSORTI" partially sorts a real vector.

7.8 Results Obtained by the Numerical Method

Numerical evaluations of the bias and the standard deviation of I_{sc}, together with estimations of the relative contributions of the component variables to the final

variance and bias calculation, are performed. A simulation output file, containing information regarding the quantile distribution of I_{sc}, is then generated. The simulation output file may be used to gain an approximate idea concerning the normality of the distribution of I_{sc}. Considering the 95% C.I., the values of $\bar{I}_{sc} + 1.96\ S_{I_{sc}}$ and $\bar{I}_{sc} - 1.96\ S_{I_{sc}}$, as calculated, are compared with the quantile 97.5% and the quantile 2.5% values of I_{sc}, respectively. If they match fairly closely, it can be said that the distribution is normal. The numerical results, obtained by means of data from different runs, are listed in Tables 11 and 12. Similar results are also obtained for the calculation of the breakthrough recovery, R_{bt}, using data from Run 6, and are listed in Table 14. Experimental results from the three replicate Runs, viz., 2, 3 and 4, are listed in Table 13.

7.8.1 Results Obtained for the Calculation of I_{sc}

Table 11 has been generated by using data from Run 1. Listed in Table 11 are the total bias and the standard deviation in the calculation of I_{sc}, together with the relative contributions of the ten different variables to the final bias and variance estimation. Using the same values of the estimated standard deviations of the component variables as in Table 11, Table 12 was generated by using the data from Run 2.

It can be seen, from Tables 11 and 12, that the total bias in the calculation of I_{sc} is quite small and the average standard deviation of I_{sc} is about 1% of its mean value. Also, it is to be noted that the major contributions to the variance of I_{sc} appear from the estimation of V_5 (which is the total volume of oil measured to establish the residual oil saturation) and V_3 (the bulk volume of the core), with their average contributions being about 48% and 44%, respectively. The error in estimating the length of the core contributes about 4.4% to the estimated variance of I_{sc}. It can be seen, from the simulation output file in Table 11, that the distribution of I_{sc} may be considered to be

Table 11: Results Obtained by the Numerical Method Using Data from Run 1

Factor	Unit	Mean	Std.Dev.	% Bias	% Var
μ_w	cp	1.028	0.005	0.0	0.0
Q	cc/hr	560.00	0.05	-0.0	0.0
Q_w	cc/hr	560.00	0.05	0.0	0.0
ΔP_1	psi	26.47	0.01	23.0	0.2
Q_0	cc/hr	560.00	0.05	0.0	0.0
ΔP_2	psi	4.02	0.01	40.5	0.0
L	cm	99.0	0.1	89.7	4.8
V_3	cc	3100	10	42.9	47.7
A_c	dyne/cm^2	16341	10	-46.3	0.4
V_5	cc	782	5	-49.7	46.9

Total Bias in instability number -0.749209

Estimated instability number 96.3845

Standard Deviation of instability number 0.908678

SIMULATION OUTPUT FILE

Quantile 0.5%	instability number	94.854
Quantile 0.1 %	instability number	95.073
Quantile 2.5%	instability number	95.421
Quantile 5.0%	instability number	95.711
Quantile 95.0%	instability number	98.641
Quantile 97.5 %	instability number	98.942
Quantile 99.0%	instability number	99.181
Quantile 99.5%	instability number	99.451

Table 12: Numerical Results Using Data from Run 2

Factor	Unit	Mean	Std.Dev.	% Bias	% Var
μ_w	cp	1.028	0.005	0.0	0.0
Q	cc/hr	50.00	0.05	0.0	1.0
Q_w	cc/hr	50.00	0.05	-26.7	0.0
ΔP_1	psi	5.80	0.01	20.9	3.2
Q_0	cc/hr	140.00	0.05	-1.4	0.1
ΔP_2	psi	0.34	0.01	64.9	1.5
L	cm	99.0	0.1	-2.8	4.0
V_3	cc	3100	10	45.7	40.6
A_c	dyne/cm^2	16341	10	-0.0	0.4
V_5	cc	705	5	-0.6	49.2
Total Bias in instability number			-0.0725368		
Estimated instability number			8.33484		
Standard Deviation of instability number			0.0850364		

Table 13: Experimental Results from the Three Replicate Runs 2, 3 and 4

Variables	Units	Run 2	Run 3	Run 4
μ_w	cp	1.028	1.028	1.028
Q	cc/hr	50.00	50.00	50.00
Q_w	cc/hr	50.00	50.00	50.00
ΔP_1	psi	5.80	-	5.87
Q_0	cc/hr	140	140	140
ΔP_2	psi	0.34	-	0.34
L	cm	99.0	99.0	99.0
V_3	cc	3100	3100	3100
A_c	dyne/cm^2	16341	16341	16341
V_5	cc	705	724	716
I_{sc}	dimensionless	8.41	-	8.38
R_{bt} (observed)	% of IOIP	50.00	49.90	49.89

Table 14: Numerical Results from Run 6

Factor	Unit	Mean	Std.Dev.	% Bias	% Var
Z_0	cm	50	5	31.4	97.0
L	cm	100	0.1	31.4	0.0
V_4	cc	983	5	-2.6	1.0
V_5	cc	760	5	-0.0	1.6
Q_0	cc/hr	560	0.05	-2.6	0.0
ΔP_1	psi	26.7	0.01	41.2	0.0
Q_w	cc/hr	100	0.05	-2.6	0.0
ΔP_2	psi	0.7	0.01	3.8	0.4

Total Bias in Breakthrough Recovery	0.62217×10^{-3} of IOIP
Estimated Breakthrough Recovery	0.512 of IOIP
Standard Deviation of Breakthrough Recovery	0.02657 of IOIP

normal. The calculated mean and standard deviation of I_{sc} are 96.3845 and 0.908678, respectively, so that $\bar{I}_{sc} + 1.96\ S_{I_{sc}} = 98.1655$ and $\bar{I}_{sc} - 1.96\ S_{I_{sc}} = 94.6035$. These values match fairly closely (within about 0.8%) with the quantile 97.5% and the quantile 2.5% values of I_{sc}, respectively.

It is demonstrated in Table 13 that, for replicate Runs 2 and 4, calculated values of I_{sc} are 8.41 and 8.38, respectively, so that the range between the two I_{sc} values is 0.03. Now, when the observed range in a sample of two items is 0.03, the central estimate of the standard deviation ($\sigma_{50\%}$) may be shown to be [49] (0.03) (0.886) = 0.02658. The 99% confidence limits for the standard deviation would be $\sigma_{99.5\%}$ = 0.03/3.97 and $\sigma_{0.5\%}$ = 0.03/0.01; that is, 0.00756 and 3.000, respectively. If the total standard deviation in the estimation of I_{sc}, based on two replicate runs, is denoted by σ_T, then it may be shown that

$$\sigma_T = \sqrt{\sigma_{GP}^2 + \sigma_M^2} \tag{136}$$

where σ_{GP} is the variability due to geological properties of the sand and the packing procedure and σ_M is found to be about 0.085. Hence, substituting $\sigma_{50\%}$ for σ_T in Equation 136, it is observed that σ_{GP}^2 has a negative value. Therefore, it may be concluded that either the maximal possible value of σ_{GP} is zero, or the value of σ_M has been over-estimated in the analysis. A similar conclusion may be reached by substituting $\sigma_{99.5\%}$ for σ_T in Equation 136. However, when $\sigma_{0.5\%}$ is substituted for σ_T in Equation 136, it may be seen that the order of magnitude of σ_{GP} is much higher than that of σ_M. Thus, it may be concluded that, considering a probability of 50%, and based on data from two replicate runs, the variability due to packing and geological properties of the sand is of a smaller order of magnitude than the measurement variability.

7.8.2 Results Obtained for the Calculation of R_{bt}

Table 14 has been generated by using data from Run 6. Listed in Table 14 are the total bias and the standard deviation in the calculation of stable R_{bt}, together with the relative contributions of the eight different variables to the final bias and variance estimation. It can be seen from Table 14 that the total bias in the calculation of R_{bt} is quite small, even though the standard deviation of R_{bt} is as high as about 5% of its mean value. This is so because of the high value of the estimated standard deviation of Z_o, as can be observed from the contribution of the Z_o term to the variance of R_{bt}, which is about 97%. The effect of the magnitude of the standard deviation of Z_o on the standard deviation of I_{sc} may be demonstrated by reducing the standard deviation of Z_o to 2% of its mean value when the standard deviation of R_{bt} comes down to about 1.36% of its average value.

It may be seen from Table 13 that, for the three replicate runs considered, the range of R_{bt} is 0.11. Now, when the observed range in a sample of three items is 0.11, the central estimate of the standard deviation ($\sigma_{50\%}$) may be shown to be [49] (0.11) (0.591) = 0.06501. The 99% confidence limits for the standard deviation would be $\sigma_{99.5\%}$ = 0.11/4.42 and $\sigma_{0.5\%}$ = 0.11/0.13; that is, 0.02489 amd 0.84615, respectively. Considering that the total standard deviation in the estimation of R_{bt}, based on three replicate runs, is comprised of the variability due to geological properties of the sand and the packing procedure, and the variability due to measurement of the variables of interest, the total standard deviation, σ_T, may be expressed by Equation 136. From Table 14, σ_M is found to be 2.657 and hence, substituting $\sigma_{50\%}$ for σ_T in Equation 136, it is observed that σ^2_{GP} has a negative value. Similar conclusions are also reached by substituting $\sigma_{99.5\%}$ or $\sigma_{0.5\%}$ for σ_T in Equation 136. Hence, it may be concluded that, either the value of σ_M is over-estimated (probably because of the high

value of the estimated standard deviation of Z_o, as shown in Table 14), or, based on a 99% confidence limit, σ_{GP} is of a much smaller order of magnitude than σ_M.

7.9 Discussion

The analytical and numerical error analysis, as performed in the present study, is based on the use of Equations 105 and 106. These equations have been developed with the assumption that all of the component variables are statistically independent. However, it is to be noted that, not all of the sixteen fundamental variables in the present study are uncorrelated. Moreover, the mean values and the standard deviations of the component variables have been estimated from data obtained from only Run1. Therefore, the results obtained from this analysis may be considered as approximate.

The numerical method yields fairly accurate results, as can be seen by comparing the standard deviation of I_{sc} obtained analytically (and given by Equation 129) with that obtained numerically (and given by Table 11). For the instability number of 97.13, the analytical method gives the value of the standard deviation of I_{sc} to be 0.9066, whereas the numerical method gives the value to be 0.9087. The major contributions to the standard deviation of I_{sc} arise out of the respective estimations of the volume of mobile oil produced from the core during waterflooding, and of the bulk volume of the core. Therefore, care must be exercised in estimating these variables.

Numerical evaluation of the standard deviation and bias in the estimation of R_{bt} has been done by using the data from Run 6, in which the waterflood was carried out at a flow rate of 100 cc/hr which resulted in an instability number just outside the stability boundary. The estimated stable breakthrough recovery from the numerical method is 0.512 of IOIP, which is within about 2.5% of the predicted or the actual stable breakthrough recovery for the fluid pair of MCT-5 and water. For the entire range of stable R_{bt}, the standard deviation is about 5% of the mean value of R_{bt}; that is, the 95% C.I. for stable R_{bt} will be approximately 0.460 and 0.564 of IOIP, for MCT-5 and

water. The fact that every calculated stable R_{bt} value for this particular fluid system is actually within this confidence limit shows that the measurement variability is of a much larger magnitude than the variability due to the sand properties and the packing procedure, and/or the value of the measurement variability has been overestimated.

SUMMARY AND CONCLUSIONS

A dimensionless scaling group for immiscible displacements in cylindrical porous media has been derived along with its critical value at the onset of instability. This was achieved by deriving the partial differential equation which describes approximately the evolution of the two-dimensional pseudointerface separating oil from water. The theory presented in this study, like that in an earlier approach [19], is based on the concept of a force potential, and hence can take into account the relative widths of the oil and water fingers. The stability boundary developed in this theory has been validated by means of experimental data. Moreover, it has been shown that the theory can be used to predict the breakthrough recovery for stable and pseudostable displacements.

Furthermore, an error analysis has been performed on the calculations of the instability number and the breakthrough recovery. For single determinations of the instability number and the breakthrough recovery, this analysis has been used to calculate the total bias and variance and also the relative contribution of each of the different component variables to the final bias and variance. Also, the contribution of the variability due to the geological properties of the sand and the packing procedure, to the total variability in the estimation of the instability number and the breakthrough recovery, has been estimated, by using data from three replicate runs.

Based on the experimental results presented herein, and keeping in mind the limitations of the theory and of the error analysis, the following conclusions may be drawn:

1. The stability boundary may be predicted by using Equation 84. Consequently, it may be concluded that Equation 87 may be used to predict the pseudointerfacial tension associated with the pseudosurface separating the two immiscible fluids.

2. The viscous fingers are initiated at a distance of about 50 cm from the inlet end of the coreholder for the particular sand-fluid system used in this study. Also, Equation 92 may be used to estimate the breakthrough recovery for a stable displacement.

3. Equation 95 may be used to estimate the breakthrough recovery for a pseudostable displacement. However, this conclusion is tentative because of the scarcity of supporting data.

4. Based on the limited amount of data available, the instability number coinciding with the onset of the pseudostable behaviour was observed to be about 450. This value of the instability number was found to correspond to a most probable mode number of 3, irrespective of the diameter of the core.

5. The variables which contribute most to errors in the estimation of the instability number and the breakthrough recovery are the total volume of mobile oil produced during waterflooding, the core bulk volume and the distance from the inlet end of the core where fingering is initiated.

6. Based on a probability of at least 50%, the variability due to the geological properties of the sand and the packing procedure has a smaller order of magnitude than the measurement variability, for the estimation of the instability number and the breakthrough recovery.

SUGGESTIONS FOR FUTURE STUDY

The following improvements are suggested in future studies:

1. Displacements should be conducted using high-flow-rate pumps, so that even for fluid pairs having low viscosity contrasts, such as MCT-5 and water, the pseudostable displacement regime might be reached. This would enable better identification of the pseudostable boundary.
2. A hydraulic ram should be constructed for the coreholder being used, in order to extract the cores from the coreholder in a more efficient manner. This would help in increasing the accuracy of measurement of the distance from the inlet end of the core where fingering is initiated.
3. An attempt should be made to design experiments with a view to obtaining detailed physical information regarding the nature of the capillary fringe separating the displacing fluid from that which is being displaced.
4. As flow in the immediate vicinity of a wellbore is radial in nature, a similar stability analysis for a plane-radial system should be undertaken.
5. An attempt should be made to extend this stability analysis in order to include non-Newtonian fluids.

REFERENCES

1. Rachford, H.H., Jr.: "Instability in Water Flooding Oil from Water-Wet Porous Media Containing Connate Water"; Soc. Pet. Eng. J., (1964), Vol. 231, 133.

2. Hagoort, J.: "Displacement Stability of Water Drives in Water-Wet Connate-Water-Bearing Reservoirs"; Soc. Pet. Eng. J., (1974), Vol. 257, 63.

3. Yortsos, Y.C. and Huang, A.B.: "Linear Stability Analysis of Immiscible Displacement: Part I - Simple Basic Flow Profiles"; SPE Res. Eng., (July, 1986), 378.

4. Jerauld, G.R., Davis, H.T. and Seriven, L.E.: "Stability of Fronts of Permanent Form in Immiscible Displacement"; SPE Paper No. 13164.

5. Taylor, G.I.: "The Instability of Liquid Surfaces When Accelerated in a Direction Perpendicular to Their Planes. I"; Proc. Roy. Soc. London, (1950), Vol. 20, 192.

6. Lewis, D.J.: "The Instability of Liquid Surfaces When Accelerated in a Direction Perpendicular to Their Planes. II"; Proc. Roy. Soc. London, (1950), Vol. 202A, 81.

7. Hill, S.: "Channelling in Packed Columns"; Chem. Eng. Sci., (1952), Vol. 1, No. 6, 247.

8. Engelberts, W.F. and Klinkenberg, L.J.: "Laboratory Experiments on the Displacements of Oil by Water from Rocks of Granular Materials"; Third World Pet. Cong. (1951), Part II, 544.

9. van Meurs, P.: "The Use of Transparent Three-Dimensional Models for Studying the Mechanism of Flow Processes in Oil Reservoirs"; *Trans.* AIME, (1957), Vol. 210, 295.

10. Bellman, R. and Pennington, R.H.: "Effects of Surface Tension and Viscosity on Taylor Instability"; Quart. Appl. Math. (1954), Vol. 12, 151.

11. Saffman, P.G. and Taylor, G.I.: "The Penetration of a Fluid into a Porous Medium or Hele-Shaw Cell Containing a More Viscous Liquid"; Proc. Roy. Soc. London, (1958), Vol. 245A, 312.

12. Chuoke, R.L., van Meurs, P. and van der Poel, C.: "The Instability of Slow, Immiscible, Viscous Liquid-Liquid Displacements in Permeable Media"; *Trans.* AIME, (1959), Vol. 216, 188.

13. Outmans, H.D.: "Nonlinear Theory for Frontal Stability and Viscous Fingering in Porous Media"; *Trans.* AIME (1962), Vol 225, 165.

14. Benham, A.L. and Olson, R.W.: "A Model Study of Viscous Fingering"; Soc. Pet. Eng. J., (June, 1963), 138.

15. Perkins, T.K. and Johnston, O.C.: "A Study of Immiscible Fingering in Linear Models"; Soc. Pet. Eng. J., (March, 1969), 39.

16. Gupta, S.P., Varnon, J.E. and Greenkorn, R.A.: "Viscous Finger Wavelength Degeneration in Hele-Shaw Models"; Water Resour. Res., (1973), Vol. 9, No. 4, 1039.

17. Gupta, S.P. and Greenkorn, R.A.: "An Experimental Study of Immiscible Displacement with an Unfavourable Mobility Ratio in Porous Media"; Water Resour. Res., (1974), Vol. 10, No. 2, 371.

18. Peters, E.J. and Flock, D.L.: "The Onset of Instability During Two-Phase Immiscible Displacement in Porous Media"; Soc. Pet. Eng. J., (April 1981), 249.

19. Bentsen, R.G.: "A New Approach to Instability Theory in Porous Media"; Soc. Pet. Eng. J., (October, 1985), 765.

20. Hubbert, M.K.: *The Theory of Ground-Water Motion and Related Papers*, Hafner Publishing Co., New York City, (1969), 199.

21. Scheidegger, A.E.: *The Physics of Flow Through Porous Media*, University of Toronto Press, Toronto, (1974), 75.

22. Bentsen, R.G.: "Use of Capillary Pressure Data to Estimate the 'Pseudointerfacial Tension' for Analysis of Stability of Fluid Flow in Porous Media"; AOSTRA J. of Res., (December, 1986), 213.

23. Coskuner, G.: *An Experimental Study of a New Approach to Instability in Porous Media*, M.Sc. Thesis, U. of Alberta, Edmonton, (1985).

24. Coskuner, G. and Bentsen, R.G.: "On the Development of a Functional Form for the Surface of an Immiscible Viscous Finger and the Use of this Surface in Stability Theory"; Chem. Eng. Res. Des., (January, 1987), Vol. 65, 41.

25. Coskuner, G. and Bentsen, R.G.: "A Modified Theory for Predicting Unstable Immiscible Displacements"; AOSTRA J. of Res., (June, 1986), 155.

26. Sarma, H.K. and Bentsen, R.G.: "An Experimental Verification of a Modified Instability Theory for Immiscible Displacements in Porous Media"; J. Can. Pet. Tech. (1987), Vol. 26, No. 4, 88.

27. Sarma, H.K.: *A Study of the Impact of Instability on the Immiscible Displacement of One Fluid by Another*, Ph.D. Thesis, U. of Alberta, Edmonton, (1988).

28. Churchill, R.V. and Brown, J.W.: *Fourier Series and Boundary Value Problems*, McGraw-Hill Book Co., Inc., New York City, 16-18.

29. Zachmanoglou, E.C. and Thoe, D.W.: *Introduction to Partial Differential Equations with Applications*, The Wilkins and Wilkins Co., Baltimore, 175.

30. Chester, C.R.: *Techniques in Partial Differential Equations*, McGraw-Hill Book Co., New York City, 101.

31. Sokolnikoff, I.S. and Redheffer, R.M.: *Mathematics of Physics and Modern Engineering*, McGraw-Hill Book Co., New York City, 472.

32. Peters, E.J.: *Stability Theory and Viscous Fingering in Porous Media*, Ph.D. Thesis, U. of Alberta, Edmonton (1979).

33. Churchill, R.V. and Brown, J.W.: *Fourier Series and Boundary Value Problems*, McGraw-Hill Book Co., Inc., New York City, 196-197.

34. Powers, D.L.: *Boundary Value Problems*, Academic Press, New York, 225.

35. Spiegel, M.R.: *Mathematical Handbook of Formulas and Tables*, Shaum's Outline Series, 250.

36. Churchill, R.V. and Brown, J.W.: *Fourier Series and Boundary Value Problems*, McGraw-Hill Book Co., Inc., New York City, 83.

37. Demetre, G.P.: *Scaling and Instability of Simultaneous Flow in Porous Media*, M.Sc. Thesis, U. of Alberta, Edmonton, (1980).

38. Demetre, G.P., Bentsen, R.G. and Flock, D.L.: "A Multi-Dimensional Approach to Scaled Immiscible Fluid Displacement"; J. Can. Pet. Tech., (July-August, 1982), 49.

39. Bentsen, R.G. and Saeedi, J.: "Liquid-Liquid Immiscible Displacement in Unconsolidated Porous Media"; J. Can. Pet. Tech., (January-March, 1981), 93.

40. Wiborg, R.: *Frontal Instabilities when Waterflooding at Unfavourable Viscosity Ratios*, M.Sc. Thesis, U. of Alberta, Edmonton, (1975).

41. Baird, H.J.: *Waterflood Behaviour of Viscous Oils*, M.Sc. Thesis, U. of Alberta, Edmonton, (1978).

42. Bentsen, R.G.: "On the Use of the Theory of Gibbs to Estimate the 'Pseudointerfacial Tension' for Analysis of Stability of Fluid Flow in Porous Media"; paper in preparation.

43. Peters, E.J., Broman, J.A. and Broman, W.H., Jr.: "Computer Image Processing: A New Tool for Studying Viscous Fingering in Core Floods"; SPE Res. Eng., (November, 1987), 720.

44. Hahn, G.J. and Shapiro, S.S.: *Statistical Models in Engineering*, J. Wiley and Sons, Inc., New York, (1967), 40.

45. Hahn, G.J. and Shapiro, S.S., 63.

46. Hahn, G.J. and Shapiro, S.S., 252

47. Hahn, G.J. and Shapiro, S.S., 75.

48. Abramowitz, M. and Stegun, I.A.: *Handbook of Mathematical Functions*, Dover Publications, Inc., New York, 914.

49. Keeping, E.S.: *Introduction to Statistical Inference*, D. Van Nostrand Co., Inc., New Jersey, (1962), 202.

BIBLIOGRAPHY

1. Abrams, A.: "The Influence of Fluid Viscosity, Interfacial Tension, and Flow Velocity on Residual Oil Saturation Left by Waterflood", Soc. Pet. Eng. J. (October, 1975), 437.

2. Bentsen, R.G.: "Conditions Under Which the Capillary Term May be Neglected", J. Can. Pet. Tech. (October-December, 1978), 25.

3. Bentsen, R.G. and Sarma, H.K.: "The External-Drive Method: Its Use and Abuse", AOSTRA J. of Res. (1989) 5, 61.

4. Bowman, F.: *Introduction to Bessel Functions*, Dover Publications, Inc., New York (1958), Chapters I, II and VII.

5. Buckley, S.E. and Leverett, M.C.: "Mechanism of Fluid Displacement in Sands", *Trans.* AIME (1942) 146, 107.

6. Collins, R.E.: *Flow of Fluids Through Porous Materials*, McGraw-Hill Book Company, Inc., New York (1961), Chapters 6 and 7.

7. Craig, F.F., Jr.: "Application of Laboratory Fluid Flow Experiments to Field Operations", Proc. Seventh World Petroleum Conress (1967) 3, 151.

8. Craig, F.F., Jr.: *The Reservoir Engineering Aspects of Waterflooding*, Monograph Volume 3, Henry L. Doherty Series, Society of Petroleum Engineers of AIME, New York (1971), Chapter 3.

9. de Haan, H.J.: "Effect of Capillary Forces in the Water-Drive Process", Proc. Fifth World Petroleum Congress (1959), Section II, 319.

10. Farouq Ali, S.M., Donohue, D.A.T. and Stahl, C.D.: "Fluid Flow in Porous Media – Problems in Relating Experiments to Field Projects", Proc. Seventh World Petroleum Congress (1967) 3, 159.

11. Jahnke, E. and Emde, F.: *Tables of Functions with Formulas and Curves*, Dover Publications, New York (1945), Chapter VIII.

12. Odeh, A.S.: "Effect of Viscosity Ratio on Relative Permeability", Soc. Pet. Eng. J. (1959) 216, 346.

13. Scheidegger, A.E.: "Growth of Instabilities on Displacement Fronts in Porous Media", The Phys. Fluids (January – February, 1960) Vol. 3, No. 1, 94.

14. Spanos, T.J.T. and de la Cruz, V.: "Some Stability Problems During Immiscible Displacement in a Porous Medium", AOSTRA J. of Res. (1984) Vol. 1, 63.

15. Welge, H.J.: "A Simplified Method for Computing Oil Recovery by Gas or Water Drive", *Trans.* AIME (1952) 195, 91.

16. Willhite, G.P.: *Waterflooding*, Society of Petroleum Engineers, Richardson (1986), Chapter 3.

17. Wygal, R.J.: "Construction of Models that Simulate Oil Reservoirs", Soc. Pet. Eng. J. (December, 1963), 281.

APPENDIX A

Derivation of Equation Describing the Pseudosurface Separating Oil from Water in a Cylindrical System

Let us consider a small, nearly rectangular portion of the pseudosurface, lying in the r-φ plane, which separates the oil from the water. Also, let the magnitude of the vertical displacement of any point in the pseudosurface be denoted by ξ (r, θ, z), where z, the amplitude of the displacement, is a function of time. Now, let us suppose that the small element of the surface is bounded by the points (r, θ, 0), (r + dr, θ, 0), (r, + dr, θ + dθ, 0) and (r, θ + dθ, 0).

In order to obtain a differential equation for the pseudosurface, we have to identify the different forces acting on the differential element of the pseudosurface. We assume that the force due to acceleration on the surface may be neglected and that the pseudosurface is under uniform tension which is given by the pseudosurface tension, σ_e. Also, due to the change in pressure across the pseudointerface, there is a vertical force P_c acting per unit area of the surface.

Now, the net force normal to the surface of the element due to the pair of tensions on the sides of the element, of length dr each, is given by [42].

$$T_{1n} = \sigma_e \cdot \frac{1}{r} dr \left[\left(\frac{\partial \xi}{\partial \theta} \right)_{\theta + d\theta} - \left(\frac{\partial \xi}{\partial \theta} \right)_{\theta} \right] \tag{A-1}$$

Similarly, the net force normal to the surface of the element due to the pair of tensions on the two curved sides of the element, of length (r + dr) dθ each, is given by

$$T_{2n} = \sigma_e \cdot (r + dr)\, d\theta \left[\left(\frac{\partial \xi}{\partial r} \right)_{r + dr} - \left(\frac{\partial \xi}{\partial r} \right)_{r} \right] \tag{A-2}$$

In addition, there is a vertical force $P_c(r, \theta, z)\ (r + dr)\ dr\ d\theta$ acting on the pseudosurface. Taking the algebraic sum of the vertical forces yields

$$\sigma_e \cdot \frac{dr}{r} \cdot \left[\left(\frac{\partial \xi}{\partial \theta}\right)_{\theta + d\theta} - \left(\frac{\partial \xi}{\partial \theta}\right)_{\theta}\right] + \sigma_e \cdot r \cdot d\theta \left[\left(\frac{\partial \xi}{\partial r}\right)_{r + dr} - \left(\frac{\partial \xi}{\partial r}\right)_{r}\right]$$

$$+ \sigma_e\, dr\, d\theta \left[\left(\frac{\partial \xi}{\partial r}\right)_{r+dr} - \left(\frac{\partial \xi}{\partial r}\right)_{r}\right] + P_c\,(r, \theta, z)\ r\ dr\ d\theta = 0 \qquad \text{(A–3)}$$

where the term $P_c\ (r, \theta, z)\ dr\ dr\ d\theta$ has been neglected in comparison to the other terms. Upon dividing Equation (A-3) by $r\ dr\ d\theta$ and letting $dr \rightarrow 0$ and $d\theta \rightarrow 0$, it follows that

$$\sigma_e \left[\frac{1}{r^2}\frac{\partial^2 \xi}{\partial \theta^2} + \frac{1}{r}\frac{\partial \xi}{\partial r} + \frac{\partial^2 \xi}{\partial r^2}\right] + P_c\,(r, \theta, z) = 0 \qquad \text{(A–4)}$$

where $P_c\ (r, \theta, z)$, the pressure difference across the interface, depends on the curvature of the surface and σ_e is independent of location on the surface.

APPENDIX B: EXPERIMENTAL RESULTS FROM THE LITERATURE

Table: B.1

Summary of Displacement Results from Peters [32]

Water-wet system; $M = \mu_o/\mu_w = 102.5$; $\sigma = 24.3$ dyne/cm; $S_{or} = 0.27$ [39]

Run	Q (cc/hr)	I_{sc}	R_{bt} (% of IOIP)
1	2.5	1.24	43.63
2	20	9.16	41.88
3	10	3.67	43.68
4	160	69.19	35.32
5	50	19.80	40.30
6	100	38.19	41.10
7	480	307.56	30.40
8	160	76.77	32.22
9	200	67.06	30.89
10	240	113.20	34.69
11	1120	585.33	23.94
12	480	191.86	26.81
13	480	211.47	33.24
14	800	286.26	28.62
15	1120	433.07	23.43

Table: B.2

Summary of Displacement Results from Demetre [37]

Water-wet system; $M = \mu_o/\mu_w = 102.5$; $\sigma = 24.3$ dyne/cm; $S_{or} = 0.27$

Run	Q (cc/hr)	I_{sc}	R_{bt} (% of IOIP)
1	140	57.496	34.63
2	40	17.18	39.71
3	3.13	1.36	42.16
4	0.5	0.234	41.99
5	25	11.39	40.91
6	15	9.70	40.19
7	50	23.45	41.90
8	3.13	1.73	44.03
9	480	304.85	32.42
10	200	93.76	36.85
11	50	24.98	39.73
12	60	24.89	40.21
13	0.50	0.245	38.94
14	50	24.22	42.00

Table: B.3

Summary of Displacement Results from Wiborg [40]

Water-wet system; $M = \mu_o/\mu_w = 111.4$; $\sigma = 34.5$ dyne/cm; $S_{or} = 0.27$

Run	Q (cc/hr)	I_{sc}	R_{bt} (% of IOIP)
1	160.0	56.83	25.90
2	80.0	28.60	25.00
3	5.0	1.80	32.80
4	15.0	5.43	31.20
5	30.0	15.64	26.70
6	2.5	0.88	31.60
7	20.0	7.17	29.90
8	60.0	21.35	26.60
9	320.0	113.48	17.30

Table: B.4

Summary of Displacement Results from Baird [41]

Water-wet system; $M = \mu_o/\mu_w = 545.7$; $\sigma = 34.0$ dyne/cm; $S_{or} = 0.45$

Run	Q (cc/hr)	I_{sc}	R_{bt} (% of IOIP)
1	2.5	6.87	27.22
2	10	24.94	24.41
3	160	426.40	19.74
4	300	963.42	16.98
5	800	4224.77	16.28
6	20	115.17	25.87
7	560	283.59	16.17
8	50	129.15	20.90
9	15	75.19	23.77
10	40	93.16	25.11
11	600	2284.51	15.20
12	1120	4654.5	15.10

APPENDIX C: PROGRAM FOR SENSITIVITY ANALYSIS.

```
C       TO PROVIDE A GENERAL CODE FOR NUMERICAL VARIANCE AND BIAS
C  COMPONENT ANALYSIS PLUS SIMULATION, OF THE DOUBLE-PRECISION
C  FUNCTION "REC(X,N)". COURTESY OF PROF. W. H. GRIFFIN, DEPT. OF
C  MINERAL ENG., UNIV. OF ALBERTA, EDMONTON (DEC. 7, 1989).
C
C                  *******     OPERATION     *******
C
C       THE NUMBER OF FUNCTION ARGUMENTS "N",THE NAMES OF THESE
C  ARGUMENTS AND THEIR UNITS (FACT(I), I=1,N), THE NAME OF THE
C  FUNCTION RESULT "FRNM", THE FUNCTION RESULT UNIT "FRUNTS",
C  INITIAL VALUES FOR THE FUNCTION ARGUMENTS AND AN INITIAL
C  FUNCTION RESULT "R" ARE SET BY THE STATEMENT "R=REC(X,N)". A
C  VARIANCE AND BIAS COMPONENT ANALYSIS TABLE IS NOW WRITTEN TO
C  THE SCREEN AND THE USER IS PROMPTED FOR MODIFICATIONS OF THE
C  ARGUMENTS (X(I), I=1,N) AND THE ESTIMATED STANDARD DEVIATIONS
C  OF THESE ARGUMENTS (SDX(I), I=1,N). THE FORMAT HERE IS LIST-
C  DIRECTED, THE ORDER IS (X(I), I=1,N), (SDX(I), I=1,N) AND
C  INTERNAL VALUES ARE DOUBLE-PRECISION.
C       THE VARIANCE AND BIAS COMPONENT ANALYSIS TABLE IS THEN
C  REWRITTEN AND THE PROGRAM RECYCLES FOR POSSIBLE ARGUMENT
C  MODIFICATION. WHEN THE USER IS SATISFIED, RECYCLE IS
C  TERMINATED BY THE LIST DIRECTED "/" OPTION. THE USER IS NOW
C  PROMPTED "SIMULATE ?". AN ANSWER WITH A WORD WHOSE FIRST
C  CHARACTER IS NOT "L" WILL CAUSE ALL ARGUMENTS TO BE SIMULATED
C  AS NORMAL VARIATES. OTHERWISE, THEY WILL BE TREATED AS LOG-
C  NORMAL VARIATES. THE FINAL USER INPUT PROMPT IS FOR "DSEED ?",
C  THE STARTING DOUBLE-PRECISION NUMBER FOR PSEUDO RANDOM NUMBER
C  GENERATION. AS THIS IS ALSO LIST DIRECTED, THE "/" RESPONSE
C  WILL LEAVE "DSEED" AT ITS INTERNAL VALUE. IF THIS OPTION IS
C  NOT TAKEN, THE USER SHOULD INPUT A POSITIVE ODD NUMBER OF AT
C  LEAST 10 DIGITS TO THE RIGHT OF THE DECIMAL. THE PROGRAM NOW
C  GOES THROUGH 10000 MONTE CARLO SAMPLES OF "R=REC(X,N)",
C  WRITING EACH SAMPLE TO A FILE IN A DOUBLE-PRECISION
C  LIST-DIRECTED FORMAT TO COMPLETE PROGRAM EXECUTION.
C
      REAL*8 X(20), BIAS(20), SDX(20), VAR(20), R, SDR, TBIAS,
     1       REC
      REAL*8 XX(20), SDXX(20), DSEED
      REAL*4 SIM(1000)
      INTEGER*4 IND(8)
      INTEGER*4 N, IER, I
      EXTERNAL REC
      CHARACTER*60 SIMFLN
      CHARACTER*28 FACT(20)
      CHARACTER*15 FRNM
      CHARACTER*30 TBC, EST, SDV
      CHARACTER*7 FRUNTS
      CHARACTER*1 YES
      LOGICAL*4 LN
```

```
      COMMON /FUNC/ FRNM, FRUNTS, FACT
      DATA LN / .FALSE. /
      DATA X, BIAS, SDX, VAR, R, SDR, TBIAS, XX, SDXX /123*0.D0/
      DATA DSEED /99876321.D0/
      DATA N /20/, IND /5, 10, 25, 50, 950, 975, 990, 995/
      DATA TBC /' TOTAL BIAS IN '/
      DATA EST /' ESTIMATED     '/
      DATA SDV /' STANDARD DEV  '/
      R = REC(X,N)
   10 FORMAT (A)
   20 FORMAT (I3, 1X, A28, 2G15.8, 2F5.1)
   30 FORMAT (' #', 9X, 'FACTOR', 18X, 'MEAN    STD DEVIATION',
     1       '    % BIAS % VAR', /)
   40 WRITE (*,30)
      DO 50 I = 1, N
   50 WRITE (*,20) I, FACT(I), X(I), SDX(I), BIAS(I), VAR(I)
      WRITE (*,60) TBC, FRNM, TBIAS, FRUNTS
      WRITE (*,60) EST, FRNM, R, FRUNTS
      WRITE (*,60) SDV, FRNM, SDR, FRUNTS
   60 FORMAT (A, A, G12.6, A)
      WRITE (*,*)'INPUT X AND SDX IN LIST DIRECTED MODE'
      READ (*,*) (X(I),I=1,N), (SDX(I),I=1,N)
      DO 70 I = 1, N
        IF (XX(I) .NE. X(I) .OR. SDX(I) .NE. SDXX(I)) GO TO 80
   70 CONTINUE
      GO TO 110
   80 CALL MNVRCP(REC, X, SDX, BIAS, VAR, N, IER)
      R = 0.D0
      SDR = 0.D0
      DO 90 I = 1, N
        R = R + BIAS(I)
   90 SDR = SDR + VAR(I)
      DO 100 I = 1, N
        IF (R .NE. 0.D0) BIAS(I) = BIAS(I) * 100.D0 / R
        IF (SDR .NE. 0.D0) VAR(I) = VAR(I) * 100.D0 / SDR
        XX(I) = X(I)
        SDXX(I) = SDX(I)
  100 CONTINUE
      TBIAS = R
      R = R + REC(X,N)
      SDR = DSQRT(SDR)
      GO TO 40
  110 WRITE (*,*)'SIMULATE ?'
      READ (*,10) YES
      IF (YES .NE. 'Y') STOP
      WRITE (*,*)'NORMAL OR LOGNORMAL ?'
      READ (*,10) YES
      IF (YES .EQ. 'L') LN = .TRUE.
      WRITE (*,*)'RANDOM SEED ?'
      READ (*,*) DSEED
      WRITE (*,*)' FILE NAME FOR SIMULATION OUTPUT ?'
      READ (*,10) SIMFLN
      OPEN (7,FILE=SIMFLN)
      DO 140 J = 1, 1000
```

```
        DO 130 I = 1, N
          IF (SDX(I) .LE. 0.D0) GO TO 130
          IF (LN) GO TO 120
          X(I) = RNORM(XX(I),SDX(I),DSEED)
          GO TO 130
  120     X(I) = RLOGN(XX(I),SDX(I),DSEED)
  130   CONTINUE
  140 SIM(J) = REC(X,N)
      CALL FSORTI(SIM, 1000, IND, 8)
      DO 150 I = 1, 8
  150 WRITE (*,160)'QUANTILE',IND(I)/10.,'%', FRNM, SIM(IND(I)),
     1FRUNTS
  160 FORMAT (A, F5.1, A, A, G12.5, A)
      DO 170 I = 1, 1000
  170 WRITE (7,*) SIM(I)
      CLOSE (7)
      END
      FUNCTION DRAND(DSEED)
C COURTESY OF PROF. W. H. GRIFFIN, UNIV. OF ALBERTA, EDMONTON
      (DEC 7, 1989).
C TO PRODUCE A UNIFORM RANDOM NUMBER
      REAL*8 DSEED, D1, D2, D3
      DATA D1, D2, D3 /2147483647.D0, 2147483648.D0, 16807.D0/
      DSEED = DMOD(D3*DSEED,D1)
      DRAND = SNGL(DSEED/D2)
      RETURN
      END
      DOUBLE PRECISION FUNCTION RNORM(U,S,DSEED)
C COURTESY OF PROF. W. H. GRIFFIN, UNIV. OF ALBERTA, EDMONTON,
      (DEC 7, 1989).
C TO PRODUCE A NORMAL VARIATE OF MEAN U AND STD DEV S
      REAL*8 DSEED, U, S, A, B, W
      LOGICAL*4 SW
      DATA SW / .FALSE. /
      IF (SW) GO TO 20
   10 A = 2.D0 * DBLE(DRAND(DSEED)) - 1.D0
      B = 2.D0 * DBLE(DRAND(DSEED)) - 1.D0
      W = A * A + B * B
      IF (W .GT. 1.D0) GO TO 10
      W = DSQRT(-2.D0*DLOG(W)/W)
      RNORM = A * W * S + U
      SW = .TRUE.
      RETURN
   20 RNORM = B * W * S + U
      SW = .FALSE.
      RETURN
      END
      DOUBLE PRECISION FUNCTION RLOGN(U,S,DSEED)
C COURTESY OF PROF. W. H. GRIFFIN, UNIV. OF ALBERTA, EDMONTON
      (DEC 7, 1989).
C TO PRODUCE A LOGNORMAL OF MEAN U AND STD DEV S
      REAL*8 U, S, DSEED, RLGN
      RLGN = DLOG(((S*S)/(U*U)) + 1.D0)
      RLGN = RNORM(DLOG(U) - RLGN/2.D0,DSQRT(RLGN),DSEED)
```

```
      RLOGN = DEXP(RLGN)
      RETURN
      END
      SUBROUTINE MNVRCP(FX, X, SDX, BIAS, VAR, N, IER)
C COURTESY OF PROF. W. H. GRIFFIN, UNIV. OF ALBERTA, EDMONTON
      (DEC 7, 1989).
      REAL*8 X(*), SDX(*), BIAS(*), VAR(*), H, FM2, FM1, F, FP1,
     1       FP2, D1, D2, FX
      REAL*8 D1L, D1R
      INTEGER*4 N, IER, I
C TESTS FOR INVALID "N" OR "SDX"
      IER = 1
      IF (N .LT. 1) RETURN
      IER = 2
      DO 10 I = 1, N
        IF (SDX(I) .LT. 0.D0) RETURN
   10 CONTINUE
      IER = 0
C LOOP FOR "BIAS" AND "VAR" EVALUATION VIA PARTIAL DERIVATIVES.
      DO 20 I = 1, N
        BIAS(I) = 0.D0
        VAR(I) = 0.D0
C IF "SDX(I)" IS 0. THEN BOTH "BIAS(I)" AND "VAR(I)" ARE 0.
        IF (SDX(I) .EQ. 0.D0) GO TO 20
C SET THE SPACING INTERVAL AND CALCULATE THE VALUE OF "FX" AT
C FIVE POINTS CENTRALLY LOCATED ABOUT "X(I)".
        H = SDX(I) / 100.D0
        X(I) = X(I) - 2.D0 * H
        FM2 = FX(X,N)
        X(I) = X(I) + H
        FM1 = FX(X,N)
        X(I) = X(I) + H
        F = FX(X,N)
        X(I) = X(I) + H
        FP1 = FX(X,N)
        X(I) = X(I) + H
        FP2 = FX(X,N)
        X(I) = X(I) - 2.D0 * H
        D1 = ((FM2 - FP2) + 8.D0*(FP1 - FM1)) / (12.D0*H)
C CALCULATE THE FIRST ORDER PARTIAL TO THE LEFT AND RIGHT OF
C CENTRE. IF EITHER IS ZERO OR OF DIFFERING SIGN THEN SET THE
C SECOND ORDER PARTIAL TO ZERO. OTHERWISE CALCULATE THE SECOND
C ORDER PARTIAL FROM THE FIVE POINTS EVALUATED.
        D1L = -3.D0 * FM2 - 10.D0 * FM1 + 18.D0 * F - 6.D0 *
     1  FP1 + FP2
        D1R = -FM2 + 6.D0 * FM1 - 18.D0 * F + 10.D0 * FP1 +
     1  3.D0 * FP2
        IF (D1L*D1R .LE. 0.D0) THEN
          D2 = 0.D0
        ELSE
          D2 = (-(FM2 + FP2) + 16.D0*(FM1 + FP1) - 30.D0*F) /
     1     (12.D0 * H ** 2)
        END IF
C BIAS COMPONENT IS ONE HALF THE PRODUCT OF THE SECOND ORDER
```

```
C PARTIAL AND THE SQUARE OF THE STANDARD DEVIATION.
C VARIANCE COMPONENT IS THE PRODUCT OF THE FIRST ORDER PARTIAL
C AND THE STANDARD DEVIATION SQUARED.
        BIAS(I) = (D2/2.D0) * (SDX(I)**2)
        VAR(I) = (D1*SDX(I)) ** 2
   20 CONTINUE
      RETURN
      END
      SUBROUTINE FSORTI(A, N, IND, NI)
C  FROM HERE ON THE CODE IS SIMILAR TO THAT GIVEN ON PAGE 410
C  P 2-0 OF COLLECTED ALGORITHMS FROM ACM VOL II.
C  COURTESY OF PROF. W. H. GRIFFIN, DEPT. OF MINERAL ENGG.,
C  UNIV. OF ALBERTA, EDMONTON (DEC 7, 1989).
C     INPUT:
C          A - A REAL VECTOR TO BE PARTIAL SORTED
C          N - THE DIMENSIONS OF THE REAL VECTOR. INTEGER
C              VARIABLE OR CONSTANT GREAT OR EQUAL TO 1
C          IND - THE ORDER STATISTIC SET THAT THE REAL VECTOR IS
C              TO PARTIALLY SORTED INTO. INTEGER VECTOR WHOSE
C              VALUES MUST BE GREATER THAN ZERO, LESS OR EQUAL
C              TO N AND ALL DIFFERENT. THEY MUST BE IN ASCENDING
C              ORDER.
C          NI - THE DIMENSIONS OF IND. INTEGER VARIABLE OR
C              CONSTANT GREATER THAN ZERO, LESS THAN OR EQUAL TO
C              N
C     OUTPUT:
C          A - THE REAL VECTOR IS REORDERED AS PER THE NI ITEMS
C              OF IND, THAT IS, A(IND(I)),I=1,NI IS IN THE
C              (IND(I)) NTH ORDERED POSITION
C          N,NI & IND - REMAIN UNCHANGED
C     SUBROUTINES REQUIRED: NONE
C
      REAL A(*), T, TT
      INTEGER N, IND(*), NI, INDU(16), INDL(16), IU(16), IL(16)
      INTEGER P, JL, JU, I, J, M, K, IJ, L
C
C     INTERNAL VARIABLES:
C          T,TT - TEMPORARY REAL STORAGE FOR A SWITCHING
C          INDU,INDL,IU,IL - INDEXING VECTORS TO ACT AS POINTERS
C                THESE VECTORS ARE DIMENSIONED AT 16 AND
C                THEREFORE LIMIT THE VALUE OF INPUT PARAMETER N
C                TO 2**(16+1) = 131072
C           I,J,M,K,P,JL,JU & IJ- INTEGER INDEXING AND TEMPORARY
C                STORAGE VARIABLES
C
      IF (NI .LT. 1 .OR. NI .GT. N) RETURN
      M = IND(1)
      IF (M .LT. 1 .OR. M .GT. N) RETURN
      IF (NI .EQ. 1) GO TO 20
      DO 10 I = 2, NI
        IF (IND(I) .LE. M .OR. IND(I) .GT. N) RETURN
   10 M = IND(I)
   20 CONTINUE
C
```

```
      JL = 1
      JU = NI
      INDL(1) = 1
      INDU(1) = 1
C
      I = 1
      J = N
      M = 1
   30 IF (I .GE. J) GO TO 140
C
C FIRST ORDER A(I),A(J),A((I+J)/2),AND USE MEDIAN TO SPLIT DATA
C
   40 K = I
      IJ = (I + J) / 2
      T = A(IJ)
      IF (A(I) .LE. T) GO TO 50
      A(IJ) = A(I)
      A(I) = T
      T = A(IJ)
   50 L = J
      IF (A(J) .GE. T) GO TO 70
      A(IJ) = A(J)
      A(J) = T
      T = A(IJ)
      IF (A(I) .LT. T) GO TO 70
      A(IJ) = A(I)
      A(I) = T
      T = A(IJ)
      GO TO 70
   60 A(L) = A(K)
      A(K) = TT
   70 L = L - 1
      IF (A(L) .GT. T) GO TO 70
      TT = A(L)
C
C    SPLIT THE DATA INTO A(I TO L).LT.T, A(K TO J) .GT.T
C
   80 K = K + 1
      IF (A(K) .LT. T) GO TO 80
      IF (K .LE. L) GO TO 60
      INDL(M) = JL
      INDU(M) = JU
      P = M
      M = M + 1
C
C    SPLIT THE LARGER OF THE SEGMENTS
C
      IF (L - I .LE. J - K) GO TO 110
      IL(P) = I
      IU(P) = L
      I = K
C
C     SKIP ALL SEGMENTS NOT CORRESPONDING TO AN ENTRY IN IND
C
```

```
   90 IF (JL .GT. JU) GO TO 140
      IF (IND(JL) .GE. I) GO TO 100
      JL = JL + 1
      GO TO 90
  100 INDU(P) = JL - 1
      GO TO 150
  110 IL(P) = K
      IU(P) = J
      J = L
  120 IF (JL .GT. JU) GO TO 140
      IF (IND(JU) .LE. J) GO TO 130
      JU = JU - 1
      GO TO 120
  130 INDL(P) = JU + 1
      GO TO 150
  140 M = M - 1
      IF (M .EQ. 0) RETURN
      I = IL(M)
      J = IU(M)
      JL = INDL(M)
      JU = INDU(M)
      IF (JL .GT. JU) GO TO 140
  150 IF (J - I .GT. 10) GO TO 40
      IF (I .EQ. 1) GO TO 30
      I = I - 1
  160 I = I + 1
      IF (I .EQ. J) GO TO 140
      T = A(I + 1)
      IF (A(I) .LT. T) GO TO 160
      K = I
  170 A(K + 1) = A(K)
      K = K - 1
      IF (T .LT. A(K)) GO TO 170
      A(K + 1) = T
      GO TO 160
      END
C
C
      DOUBLE PRECISION FUNCTION REC(X,N)
C       FUNCTION FOR CALCULATING THE INSTABILITY NUMBER FOR A
C  CYLINDRICAL SYSTEM WHICH IS A DIMENSIONLESS NUMBER. THIS NO.
C  AND ITS STANDARD DEVIATION ARE CALCULATED USING THE VALUES AND
C  THE STANDARD DEVIATIONS OF THE FUNDAMENTAL MATERIAL AND
C  EXPERIMENTAL VARIABLES.
C
C INPUT: X(1)=REAL*8 VARIABLE GIVING THE WATER VISCOSITY
C        cp
C        X(2)=REAL*8 VARIABLE GIVING THE FLOW RATE
C        cc/hr
C        X(3)=REAL*8 VARIABLE GIVING THE WATER FLOW RATE
C        cc/hr
C        X(4)=REAL*8 VARIABLE GIVING THE PRESSURE DROP(1)
C        psi
C        X(5)=REAL*8 VARIABLE GIVING THE FLOW RATE OF OIL
```

```
C         cc/hr
C         X(6)=REAL*8 VARIABLE GIVING THE PRESSURE DROP(2)
C         psi
C         X(7)=REAL*8 VARIABLE GIVING THE LENGTH
C         cm
C         X(8)=REAL*8 VARIABLE GIVING THE BULK VOL
C         cc
C         X(9)=REAL*8 VARIABLE GIVING THE AREA UNDER THE CAPILLARY
C         CURVE dyne/cm**2
C
C         X(10)=REAL*8 VARIABLE GIVING THE VOLUME OF OIL THAT
C         COMES OUT OF THE CORE cc
C
      REAL*8 X(*)
      INTEGER*4 N
      CHARACTER*28 FACT(20)
      CHARACTER*15 FRNM
      CHARACTER*7 FRUNTS
      COMMON /FUNC/ FRNM, FRUNTS, FACT
      LOGICAL*4 SW
      DATA SW / .FALSE. /
      IF (SW) GO TO 10
      FRNM = 'Inst. number'
      FRUNTS = 'non dim'
      FACT(1) = 'H2O visco cp'
      FACT(2) = 'Dis rate cc/hr'
      FACT(3) = 'H2O rate cc/hr'
      FACT(4) = 'Delta P1 psi'
      FACT(5) = 'Oil rate cc/hr'
      FACT(6) = 'Delta P2 Psi'
      FACT(7) = 'Length cm'
      FACT(8) = 'Bulk vol cc'
      FACT(9) = 'Ac dyne/cm2'
      FACT(10) = 'Oil vol cc'
C
      X(1) = 1.028D0
      X(2) = 560.D0
      X(3) = 560.0D0
      X(4) = 26.47D0
      X(5) = 560.D0
      X(6) = 4.02D0
      X(7) = 99.D0
      X(8) = 3100.D0
      X(9) = 16341.D0
      X(10) = 782.D0
C
      N = 10
      SW = .TRUE.
C     U = End-point mobility ratio
   10 U = X(3) * X(4) / (X(5)*X(6))
C     V = Correction factor, which is a function of mobility
C         ratio
      V = ((U**.66666666666667D0) + 1.D0) /
     #((U**.666666666667D0)*2.D0)
```

```
      W = (U - 1.D0) * V
C     Y = Permeability to water at residual oil saturation
      Y = X(3) * X(1) * (X(7)**2.D0) / (X(8)*X(6))
C     Z = Pseudointerfacial tension
      Z = X(9) * X(10) / X(8)
      REC = 87786.946 * X(1) * X(2) * W / (Y*Z)
      RETURN
      END
```